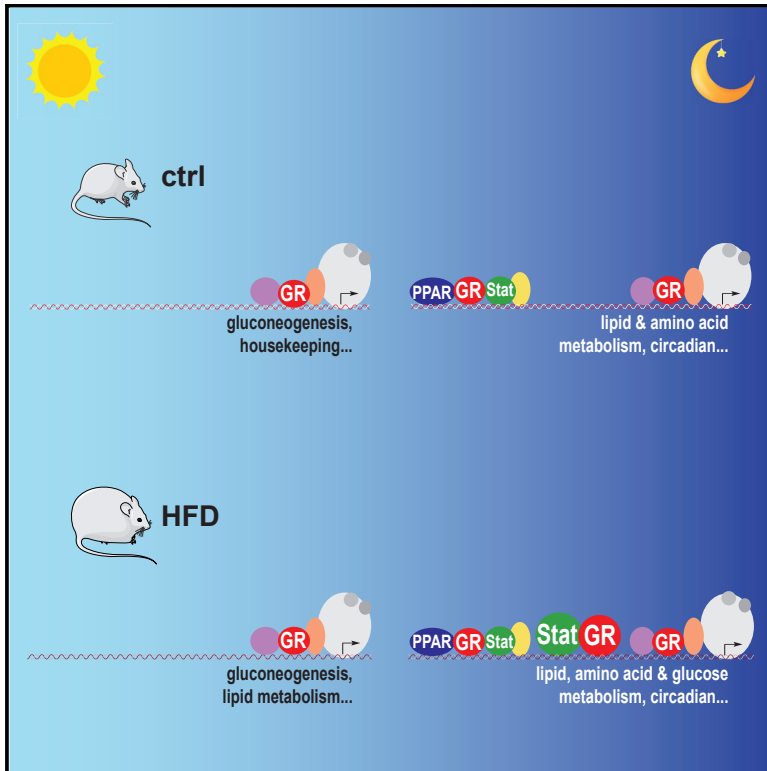


Cistronic Reprogramming of the Diurnal Glucocorticoid Hormone Response by High-Fat Diet

Graphical Abstract



Authors

Fabiana Quagliarini, Ashfaq Ali Mir, Kinga Balazs, ..., Fabian Volker Filipp, Grant Daniel Barish, Nina Henriette Uhlenhaut

Correspondence

henriette.uhlenhaut@helmholtz-muenchen.de

In Brief

Glucocorticoid hormones are secreted with a prominent daily rhythm, but their diurnal genomic actions remain uncharacterized. Quagliarini et al. show how the glucocorticoid receptor controls daily cycles of glucose and triglyceride metabolism by time-dependent chromatin binding and target gene transcription and how this rhythm is augmented by high-fat diet.

Highlights

- The glucocorticoid receptor (GR) shows rhythmic binding to chromatin in mouse liver
- The majority of diurnally oscillating transcripts are directly regulated by GR
- Hepatic GR controls circulating glucose and triglycerides during feeding and fasting
- High-fat diet (HFD) enhances GR-STAT5 co-occupancy of metabolic enhancers at night

Cistromic Reprogramming of the Diurnal Glucocorticoid Hormone Response by High-Fat Diet

Fabiana Quagliarini,^{1,2} Ashfaq Ali Mir,^{1,2} Kinga Balazs,^{1,2} Michael Wierer,³ Kenneth Allen Dyar,^{1,2} Celine Jouffe,^{1,2} Konstantinos Makris,^{1,2} Johann Hawe,⁴ Matthias Heinig,^{4,5} Fabian Volker Filipp,^{4,6} Grant Daniel Barish,^{7,8} and Nina Henriette Uhlenhaut^{1,2,9,10,*}

¹Institute for Diabetes and Obesity (IDO), Helmholtz Center Munich (HMGU) and German Center for Diabetes Research (DZD), Ingolstaedter Landstr. 1, 85764 Neuherberg (Munich), Germany

²Institute for Diabetes and Cancer (IDC), Helmholtz Center Munich (HMGU) and German Center for Diabetes Research (DZD), Ingolstaedter Landstr. 1, 85764 Neuherberg (Munich), Germany

³Department of Proteomics and Signal Transduction, Max Planck Institute of Biochemistry, 82152 Martinsried (Munich), Germany

⁴Institute of Computational Biology (ICB), HMGU, Ingolstaedter Landstr. 1, 85764 Neuherberg (Munich), Germany

⁵Department of Informatics, Boltzmannstr. 3, 85748 Garching, Technische Universitaet Muenchen (TUM), Munich, Germany

⁶School of Life Sciences Weihenstephan, Maximus-von-Imhof-Forum 3, 85354 Freising, Technische Universitaet Muenchen (TUM), Munich, Germany

⁷Department of Medicine, Division of Endocrinology, Metabolism and Molecular Medicine, Robert H. Lurie Comprehensive Cancer Center, Northwestern University Feinberg School of Medicine, Chicago, IL 60611, USA

⁸Jesse Brown VA Medical Center, Chicago, IL 60612, USA

⁹Metabolic Programming, School of Life Sciences Weihenstephan, Gregor Mendel Str. 2, 85354 Freising, Technische Universitaet Muenchen (TUM), Munich, Germany

¹⁰Lead Contact

*Correspondence: henriette.uhlenhaut@helmholtz-muenchen.de

<https://doi.org/10.1016/j.molcel.2019.10.007>

SUMMARY

The glucocorticoid receptor (GR) is a potent metabolic regulator and a major drug target. While GR is known to play integral roles in circadian biology, its rhythmic genomic actions have never been characterized. Here we mapped GR's chromatin occupancy in mouse livers throughout the day and night cycle. We show how GR partitions metabolic processes by time-dependent target gene regulation and controls circulating glucose and triglycerides differentially during feeding and fasting. Highlighting the dominant role GR plays in synchronizing circadian amplitudes, we find that the majority of oscillating genes are bound by and depend on GR. This rhythmic pattern is altered by high-fat diet in a ligand-independent manner. We find that the remodeling of oscillatory gene expression and postprandial GR binding results from a concomitant increase of STAT5 co-occupancy in obese mice. Altogether, our findings highlight GR's fundamental role in the rhythmic orchestration of hepatic metabolism.

INTRODUCTION

Circadian rhythms drive the physiological adaptation to daily phases of resting/fasting and activity/feeding (Eckel-Mahan and Sassone-Corsi, 2013; Panda, 2016). At the molecular level, the circadian clock consists of a 24-h feedback loop in which the activators CLOCK and BMAL1 (ARNTL) induce their own

repressors, CRY1/2 and PER1/2/3. A second loop is formed by the nuclear receptors REV-ERB α/β (NR1D1/2) and ROR $\alpha/\beta/\gamma$ (RORA/B/C) (Takahashi, 2017).

Glucocorticoids (GCs) are steroid hormones secreted with a prominent circadian rhythm. GCs peak at the onset of the feeding phase, occurring in the early night in rodents and the early morning in humans (Spiga et al., 2014). GCs maintain blood glucose during periods of stress or fasting and entrain metabolic programs among different organs (Patel et al., 2014). It has been shown that GCs can synchronize daily rhythmicity in peripheral tissues and that treating cells and mice with GCs induces circadian gene expression and corresponding oscillations (Balsalobre et al., 2000; Oishi et al., 2005; Reddy et al., 2007).

GCs bind to the GC receptor (GR; NR3C1), a ligand-gated transcription factor belonging to the nuclear receptor superfamily. Upon hormone binding, GR enters the nucleus to regulate gene expression by direct binding to GC response elements (GREs) in the DNA of target promoters or enhancers (Greulich et al., 2016). Several studies have shown both genetic and physical interactions between GR and the core clock machinery; functional GREs have been identified in the *Per1* and *Per2* regulatory regions, while the *Rev-erb α* promoter was found to be repressed by GR (So et al., 2009; Torra et al., 2000; Yamamoto et al., 2005). CRY1 and CRY2 were shown to interact with GR in a ligand-dependent manner to repress the activation of gluconeogenic genes like *Pck1* (Lamia et al., 2011). Similarly, CLOCK antagonizes GC-induced transcriptional activity via lysine acetylation of the GR protein itself (Nader et al., 2009).

Disruption of either clock function or GC secretion causes profound metabolic dysregulation, resulting in obesity, type 2 diabetes, and nonalcoholic fatty liver disease (Eckel-Mahan and Sassone-Corsi, 2013; Marcheva et al., 2013). On the other hand, GC excess has detrimental effects on glucose and fat

metabolism (Patel et al., 2014). Finally, there is a bifacial relationship between metabolism and the clock, as the internal time-keepers are very sensitive to changes in the nutritional environment. For instance, it has been shown that excessive caloric intake (just like time-restricted feeding) can shift circadian patterns of transcription and energetics (Damiola et al., 2000; Eckel-Mahan et al., 2013; Bass, 2016). Thus, circadian misalignment from inappropriate feeding schedules or shift work is associated with metabolic disease and altered GC rhythmicity (Barclay et al., 2012; Spiegel et al., 2009).

Despite much evidence for a role for GR in circadian biology, its actual contribution to diurnal rhythms has not been studied on a genomic scale. We used chromatin immunoprecipitation sequencing (ChIP-seq), RNA sequencing (RNA-seq), proteomics, and mouse genetics to characterize hepatic GR function around the clock. Here, we show that the daily rhythm of corticosterone secretion has a differential effect on chromatin occupancy by GR. We find that GR regulates nutrient partitioning by binding to promoter proximal sites near housekeeping and gluconeogenic genes during the day, while the nightly GC surge allows GR to reach distant enhancers activating lipid and amino acid metabolism. The majority of 24-h oscillating genes are bound by GR in a time-point-specific manner overlapping with core clock factors. Surprisingly, this rhythmic pattern is altered by nutritional challenge. Exposure to high-fat diet (HFD) causes an expansion of the GR cistrome selectively during the night. This concurs with a remodeling of target gene expression and an increased crosstalk with STAT5 signaling. By using liver-specific knockout mice, we demonstrate that these GR-dependent temporal metabolic gene programs affect circulating glucose and triglycerides respectively during feeding and fasting. Furthermore, we observe an altered response to exogenous GCs in obese mice. Taken together, we provide evidence that nutrition influences the clock and the GC response in a ligand-independent fashion.

RESULTS

GR Binding to Chromatin Is Rhythmic

To investigate the genomic extent of circadian gene regulation by GR, we performed ChIP-seq on mouse livers every 4 h throughout the day and night cycle. Our experimental cohort showed the expected rise in corticosterone levels toward zeitgeber time 12 (ZT12) (lights off), with the lowest levels being detected at ZT0 (lights on) (Figure S1A). We detected binding of GR to its known hepatic target genes, such as *Per1*, in all replicates (Figure 1A and data not shown). For our analyses, normalized ChIP-seq data from two biological replicates were used for peak calling. We then created a “peak union” of 14,920 genomic sites reproducibly bound by GR at any given time point. Subsequently, we quantified occupancy from the sequencing tag counts for all peaks within the union for each time point.

Interestingly, it appears that the strength of the ChIP-seq signal mirrored the endogenous ligand availability, with peak GR occupancy coinciding with the highest levels of hormone secretion (Figures 1A, 1B, and S1A–S1C). The highest number of GR-bound loci was found at ZT12, at the beginning of the active/feeding phase and at the peak of corticosterone secretion.

Afterward, at ZT16 and ZT20, these numbers dropped, reaching the lowest amount of GR-bound *cis*-regulatory elements during the day (ZT0, ZT4, and ZT8). GR binding largely occurred near gene bodies during this phase, meaning that high-affinity sites bound during the day under low hormone levels were primarily at the promoter. During the night (ZT12, ZT16, and ZT20), increased ligand availability seemed to enable GR to reach distant enhancers, and a larger fraction of ChIP peaks could be detected at greater distance from the transcription start site (TSS; Figures 1C and S1C). Approximately 800 GR-binding sites consistently mapped to <1 kb upstream of the TSS during both day and night, while the number of distal intergenic elements increased from <500 during the day to >2,000 at night.

To further characterize these target sites, we grouped the first three (lights on: ZT0, ZT4, and ZT8) and the last three (lights off: ZT12, ZT16, and ZT20) time points together. Figure 1D shows that most of the GR-binding sites occupied during fasting were also bound during the feeding phase. Functionally, these promoter-proximal sites corresponded to housekeeping genes involved in chromatin organization, gene expression, and cellular maintenance. Consistent with its known role in gluconeogenesis, “glucose metabolism” was an enriched term. The majority of GR sites (~10,000), which were occupied only at night and include distal elements, however, were linked to genes important for amino acid and cholesterol metabolism, fatty acid, and triglyceride metabolism. Hence, metabolic gene expression programs were regulated by GR in response to hormone specifically at night, while the mice were moving, eating, and digesting their food (Figures 1D and S1D–S1F).

Motif analyses revealed a significant enrichment for known co-occurring liver-specific transcription factors, such as HNF4 α , C/EBP, FoxA, and HNF6 (Lim et al., 2015), at all times. We also newly identified PPAR (and CREB) response elements near GREs in our cistromes. Promoter-proximal “high-affinity” sequences occupied during both day and night were further enriched for ETS transcription factor motifs and showed a higher percentage of “perfect” GREs, whereas the distal sites bound only at night additionally featured HNF1 motifs and fewer consensus GREs (Figures 1E and 1F).

In summary, our ChIP-seq experiments around the clock in mouse livers showed that GR chromatin occupancy followed a daily rhythm aligned with its ligand availability. Low hormone levels during the day resulted in promoter proximal binding near housekeeping and gluconeogenic genes, while high corticosterone during the night brought about additional binding to distal regulatory elements near lipid metabolic target genes.

GR Binding Overlaps with Core Clock Factors and Drives Rhythmic Transcription

Since GR activity is tightly connected with circadian rhythms, we integrated our datasets with published liver cistromes for the core clock machinery (Koike et al., 2012). We calculated the peak overlap for our GR ChIP sequences with CLOCK, BMAL1, PER1, PER2, CRY1, and CRY2 ChIP signals from each time point. We then performed functional annotation of co-bound promoters and enhancers by association with the nearest coding gene. As shown in Figure 2A, GR binding only partially overlapped with CLOCK and BMAL1, given that they

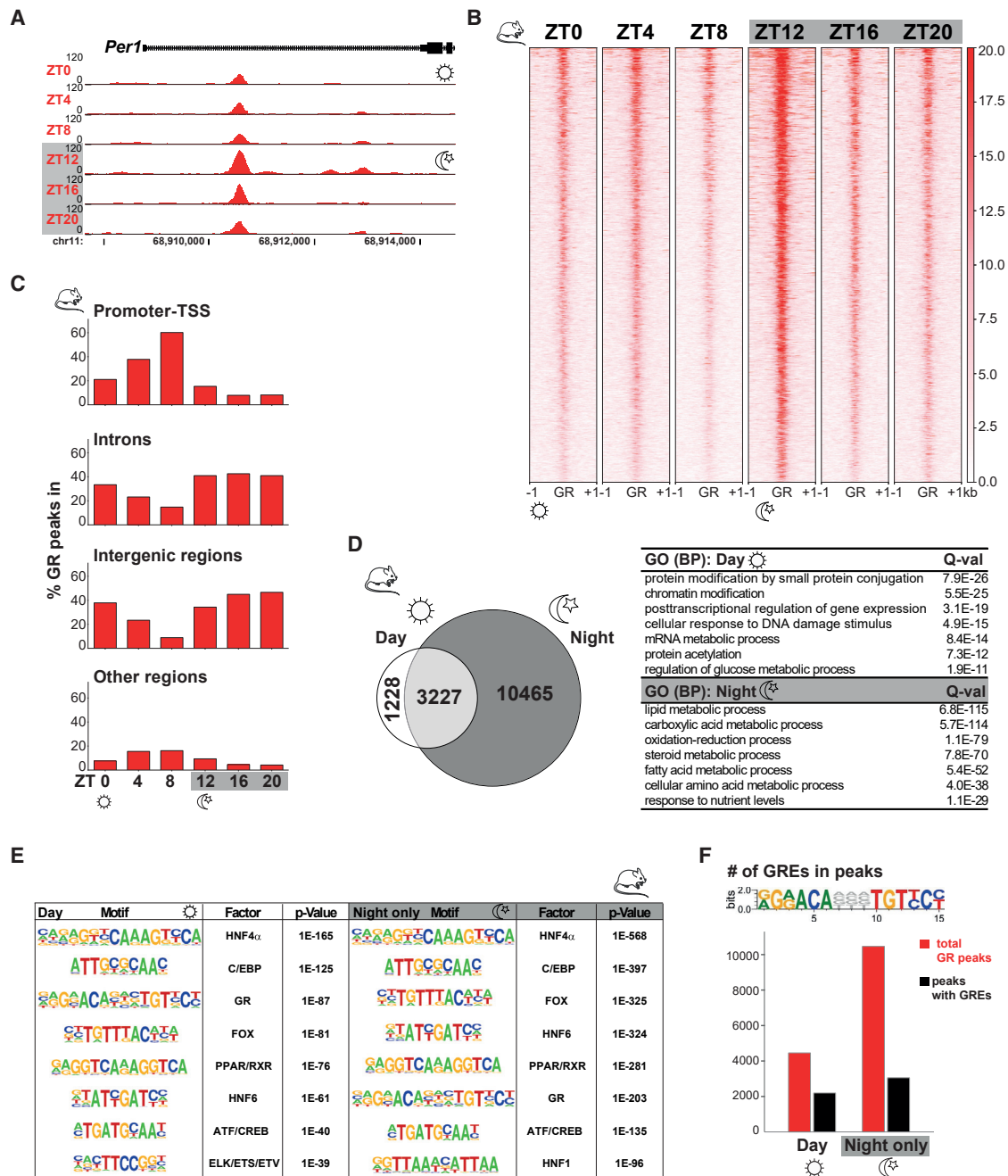


Figure 1. Differences in Genomic Binding of GR during the Day and Night Cycle in Mouse Livers

(A) GR occupancy at the *Per1* locus for ZT0, ZT4, ZT8, ZT12, ZT16, and ZT20 as determined by ChIP-seq analysis in mouse livers (normalized tag counts for one representative sample shown).

(B) Heatmap of GR genome-wide binding for ZT0–ZT20. Each row shows the normalized unique tag counts for one GR binding event (ChIP peak) of the union (sum of all reproducible peaks from two replicates for all six time points), ordered by signal strength.

(C) GR ChIP peak percent distribution over the indicated genomic regions for the six time points.

(D) Functional characterization of GR's genomic occupancy during day and night. The three time points of the light phase (ZT0, ZT4, and ZT8 = day) and the dark phase (ZT12, ZT16, and ZT20 = night) were combined into the Venn diagram. The majority of sites bound during the day (73.1%) were also bound at night. The table displays gene ontology analysis of the genes nearest to the 4,455 day binding sites and the 10,465 night-only binding sites.

(E) Motif analyses of the 4,455 day and 10,465 night-specific GR ChIP sequences for co-occurring hepatic transcription factors. Data presented is from two biological replicates per time point (i.e., a total of six samples for each day and night).

(F) Number of GREs in GR ChIP peaks for day and night, as defined by the consensus sequence shown.

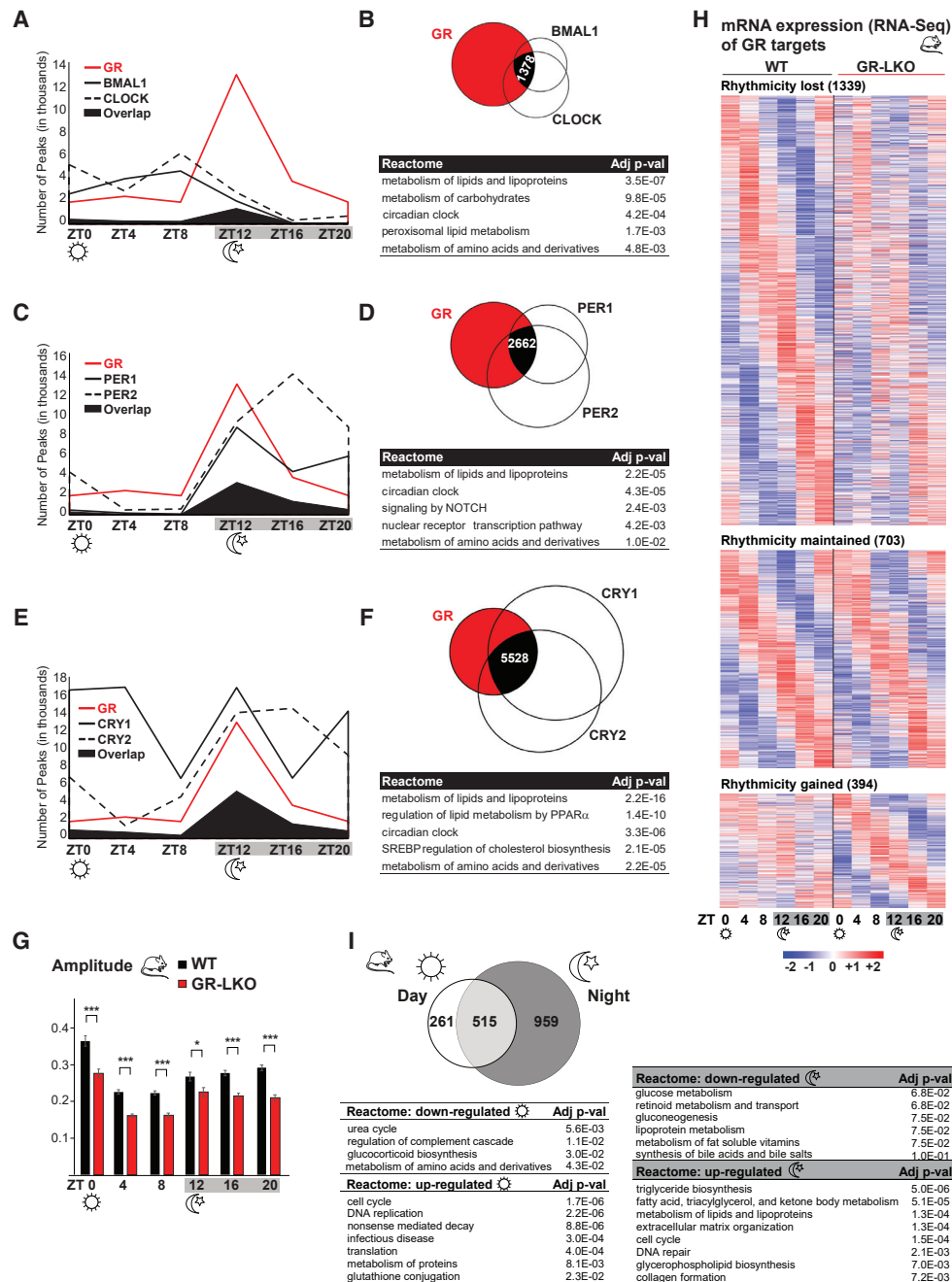


Figure 2. GR Binding Overlaps with Core Clock Factors to Generate Transcriptional Rhythms

(A, C, and E) Phase distributions, as number of peaks per time point, for GR with BMAL1/CLOCK (A), PER1/2 (C), and CRY1/2 (E); co-bound sites are solid black. (B, D, and F) Venn diagrams depict the GR union from all time points (14,920 sites) intersecting with unions for BMAL1 (6,184) and CLOCK (9,294) (B), PER1 (12,534) and PER2 (20,944) (D), and CRY1 (34,581) and CRY2 (28,658) (F). Functional annotation of *cis*-regulatory sites bound by all three factors (black) is in the tables below (Koike et al., 2012).

(G) Amplitude distribution for ZT0–ZT20 in livers from GR-liver-specific knock out (LKO) (*Alb-Cre* × *GR^{fl/fl}*) compared to *GR^{fl/fl}* littermates (WT). 3,400 genes cycling in control mice were binned according to peak time point (4 h). Values are represented as mean ± SEM (n = 3 per group).

(H) Phase-sorted heatmap of oscillating transcripts in wild-type (WT) and GR-LKO livers for ZT0, ZT4, ZT8, ZT12, ZT16, and ZT20 (n = 3).

(I) Venn diagram showing number of differentially regulated genes in GR-LKO during the day (ZT0, ZT4, and ZT8) and night (ZT12, ZT16, and ZT20). Pathway annotation was performed for transcripts either up- or downregulated in GR-LKO. *p < 0.05, ***p < 0.001 (two tailed t test).

primarily act during the day, while GR mainly appeared at night. In order to characterize commonly regulated genes, irrespective of the phase of genomic binding, we performed functional annotation of all co-bound promoters and enhancers by association with the nearest protein coding gene. The genes co-occupied in sum by GR together with CLOCK/BMAL1 were involved in carbohydrate, lipid, and amino acid metabolism, as well as circadian clock function, consistent with their roles in metabolic regulation (Figure 2B).

Both GCs and BMAL1/CLOCK are potent inducers of *Per1* and *Per2* expression. Consequently, we found co-occupancy of *cis*-regulatory elements by GR, PER1, and PER2 mostly at ZT12, ZT16, and ZT20, with GR slightly preceding *Per1/Per2* (Figure 2C). The genes commonly regulated during the night were assigned to lipid and amino acid metabolism, circadian clock function, and Notch signaling (Figure 2D). Again, this underscores the links among GCs, the clock, and metabolic homeostasis.

GR has previously been reported to physically interact with CRY1/2 in mouse livers (Lamia et al., 2011). Accordingly, we observed the largest overlap among all the clock factors for GR, CRY1, and CRY2. Similar to PER1 and PER2, GR binding coincided with cryptochromes predominantly at ZT12 and during the remainder of the dark phase (Figure 2E). Again, the gene networks that could be linked to these co-bound enhancers regulated lipid and amino acid metabolism, clock function, and Srebp targets (Figure 2F).

In addition, we used ChIP-seq datasets for REV-ERB- α/β and ROR- α/γ (Cho et al., 2012; Fang et al., 2014; Zhang et al., 2015) to determine the potential impact of GR on this regulatory loop (Figure S2A). Both REV-ERBs peak at ZT8, before being repressed by GR, while RORs peak at night (Bookout et al., 2006; Yang et al., 2006). Both REV-ERB- α/β and ROR- α/γ significantly overlapped with GR at common enhancers and promoters. GR and REV-ERB- α/β co-bound approximately 6,000 sites, of which about 5,000 sites were identically co-occupied by GR and ROR- α/γ . Of course these events did not happen simultaneously, but rather sequentially. These core *cis*-regulatory sequences targeted by GR and the Rev-erb-ROR loop again corresponded to genes involved in lipid, fatty acid, and amino acid metabolism, the circadian clock, and PPAR- α activity.

Taken together, we found that GR occupancy partially overlapped with the classical clock transcription factors, most prominently with cryptochromes and the ancillary loop, in a rhythmic pattern at loci governing glucose, lipid, and amino acid metabolism. One predominant theme among all the GR and “clock” co-occupied target genes was an enrichment for PPAR signaling (Figures 2B–2F and S2A). This concurs with the PPAR responsive element (PPARE) motifs enriched in our day and night GR cistromes (Figure 1E) and is consistent with PPAR- α ’s known role as a direct mediator of circadian lipid metabolism in the liver (Chen and Yang, 2014).

Finally, we detected GR ChIP peaks within the promoter or enhancer regions of all core clock genes (Table S1). We therefore profiled mRNA expression over 24 h in liver-specific GR knockout mice (Figures S2B and S2C). Using “JTK cycle” to identify mRNAs with robustly oscillating expression profiles, we found that loss of GR caused significant amplitude dampening of

rhythmic gene expression across all six time-points (Figure 2G). Specifically, over 1,300 rhythmic mRNAs harboring a nearby GR peak lost oscillation, despite the presence of a functional core clock (Figure 2H). In line with our ChIP-seq results, the three ‘dark’ time-points (ZT12, 16, 20) showed more differential gene regulation than the light phase in the GR mutants (Figures 2I, S2B, and S2C). Genes involved in glucose metabolism were downregulated, while lipid, fatty acid, and triglyceride metabolism was upregulated at night. Our results suggest that GR interacts with the core clock loop to generate rhythmic output, and that co-regulation of these programs is involved in daily cycles of metabolic adaptation to feeding and fasting (Figure S2D).

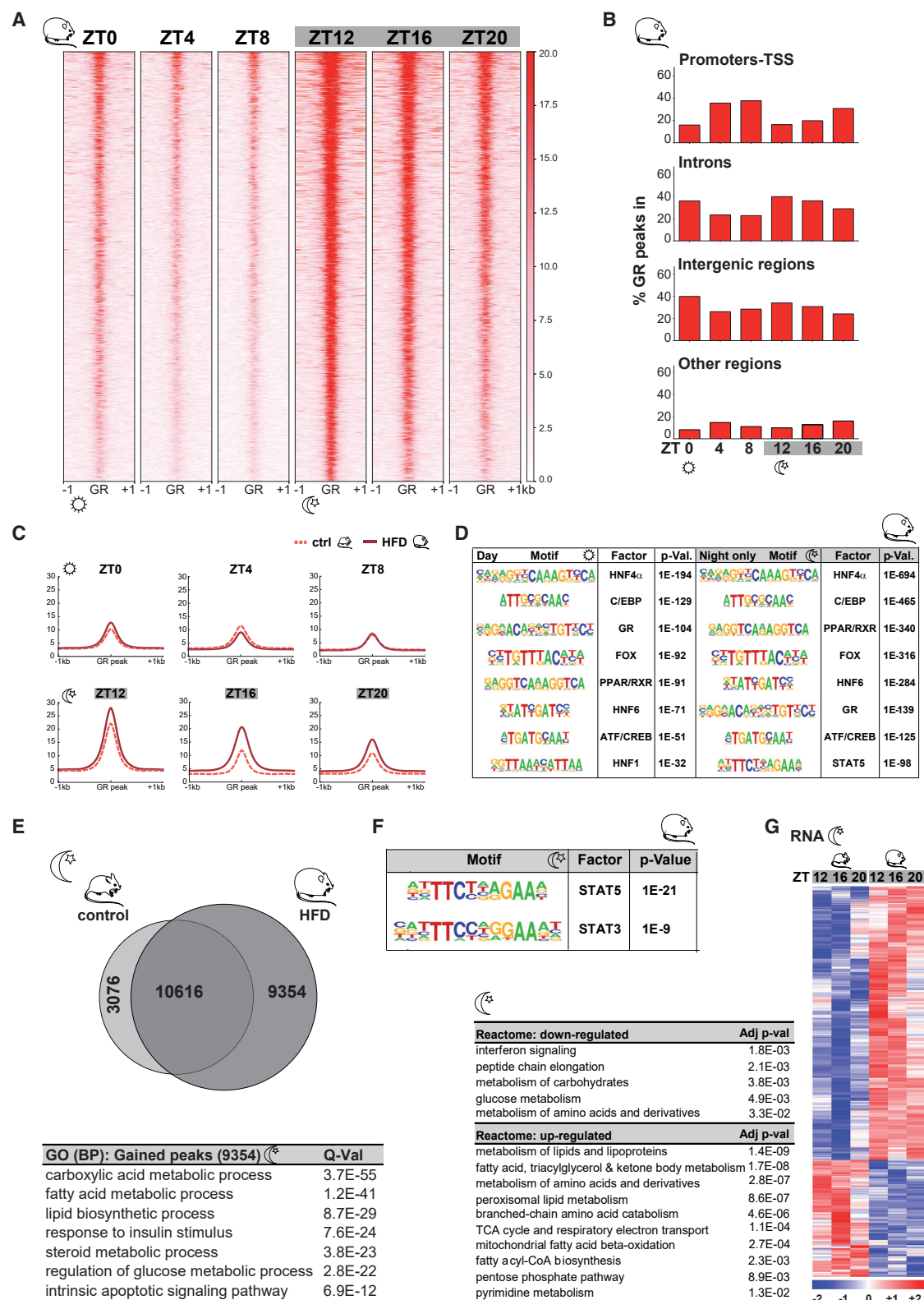
HFD Induces Cistronic Reprogramming

Prolonged HFD feeding can alter the mammalian circadian clock, for example by disrupting behavioral and molecular rhythms in mice (Kohsaka et al., 2007). We therefore performed analogous GR ChIP-seq experiments in mouse livers after 12 weeks of HFD. Importantly, we did not observe significant differences in serum corticosterone concentration in the HFD group, which showed the expected weight gain and insulin resistance (Figures S3A–S3G).

Interestingly, while the general pattern of circadian GR binding was conserved, we found a significant increase in both the number of peaks and the number of tag counts per site, most prominently at night, upon exposure to HFD (Figures 3A–3C). For example, the total number of peaks at ZT12 increased by more than 3,000. This amplified intensity of genomic GC action was mainly detected at ZT12, ZT16, and ZT20 and led to a gain of GR binding near promoters, thereby altering the normal proximal-distal distribution during the day-night cycle. Although we did not notice any alteration in signal strength during the day (ZT0, ZT4, and ZT8), we discovered a pronounced enrichment of target gene sets involved in energy metabolism, in addition to the “housekeeping” programs identified in the light phase of controls (Figures S3B and S3C). This additional lipid annotation of the rest/fasting phase in our GR cistromes could be a signature of the disrupted energy partitioning that occurs under HFD (Bass, 2016).

Both “day” (ZT0, ZT4, and ZT8) and “night” (ZT12, ZT16, and ZT20) GR cistromes were again co-enriched for liver-specific motifs such as C/EBP, HNF4 α , FoxA, and PPAR. However, the HFD group now additionally featured a STAT5 motif near GREs (Figure 3D). While ~13,000 sites were collectively bound by GR during the night in controls, HFD tissue displayed additional 9,354 GR peaks (Figure 3E). These night-specific gained GR-binding sites were associated with genes involved in both glucose and lipid or fatty acid metabolism as well as insulin signaling. A motif enrichment analysis to identify specific signatures overrepresented in only these >9,000 night-specific HFD-induced GR-binding sites again found a STAT consensus motif (Figure 3F). We would like to stress that the newly gained HFD peak sequences did contain GREs, but only the STAT motif was distinct.

RNA-seq data from the same livers displayed differential mRNA expression for several hundreds of genes near these gained peaks on HFD. Once more, the expression differences of these putative HFD-induced GR targets were more prominent



(legend on next page)

during the night and were associated with glucose, amino acid, lipid, and fatty acid metabolism (Figures 3G and S3H).

In conclusion, HFD reprogrammed hepatic GR cistromes primarily at night during the feeding phase. Increased DNA binding by GR was associated with STAT5 motifs near genes important for glucose, lipid, and fatty acid metabolism. Nightly reprogramming occurred despite similar endogenous ligand levels; similar amounts of nuclear GR, CRY1, and CRY2 proteins (Figures S3F, S3G, and S3I); and comparable mRNA profiles of *GR*, *Stat5*, and *11 β -hydroxysteroid dehydrogenase*, the gatekeeper enzyme that produces active intracellular GCs (see below).

GR, STAT5, and PPAR α Signaling Pathways Intersect

Our motif and pathway enrichment searches predicted the involvement of PPAR and STAT signaling in the modulation of GR activity. PPAR α is the most prominent PPAR in the liver, acting as a key sensor for nutritional cues such as fatty acids and lipids, and has an integral role in hepatic energy balance (Kersten et al., 1999; Preidis et al., 2017). This makes it a promising drug target for the treatment of hepatic steatosis and fibrosis (Pawlak et al., 2015). It is conceivable that HFD-fed mice show differences in effective PPAR ligand availability due to changes in diet composition or deregulation of metabolic networks.

STAT5 genetically interact with GR in liver homeostasis, and *GR* \times *Stat5* hepatocyte-specific double-mutant mice develop hepatic steatosis and hepatocellular carcinoma (Engblom et al., 2007; Mueller et al., 2011, 2012). *In vivo*, STAT5 activity is regulated by pulsatile growth hormone (GH) or cytokine signaling (Baik et al., 2011).

These observations, together with the STAT5 motif being prominently enriched in the differential GR-bound sequences, prompted us to perform ChIP-seq for both PPAR α and STAT5 in control and HFD livers at ZT12. As expected, motif analyses showed both STAT and PPAR response elements as the top enriched in the corresponding datasets, together with GREs and the typical liver signatures. Moreover, pathway annotations of the target genes for both factors were indicative of their roles as key regulators of hepatic metabolism, irrespective of diet (Figures S4A–S4D).

Interestingly, PPAR α occupancy remained largely unchanged between control and HFD livers, while STAT5 showed an increased recruitment and an increased overlap with GR on HFD (Figures 4A–4C and S4E). For example, overlap between GR and STAT5 grew from \sim 4,000 to almost 8,000 peaks upon exposure to HFD. Co-occupancy between GR and PPAR α , on the other hand, remained almost constant between 2,000 and

3,000 peaks. Figure 4D shows two examples of metabolic genes co-bound by GR, PPAR α , and STAT5, the *Pemt* and *Abat* loci. Of course, this does not mean that PPAR α transcriptional activity was not altered, i.e., via changes in ligand availability or co-regulator recruitment.

Importantly, these GR-bound *cis*-regulatory elements almost all (>98%) showed enrichment for the active histone H3K27 acetylation mark, which concomitantly increased at ZT12 (compared to ZT0) and under HFD (at ZT12, compared to control diet) (Figures 4D–4F, S4F, and S4G).

Briefly, we found an expansion of both GR and STAT5 cistromes at ZT12 in HFD livers, accompanied by increased histone H3K27 acetylation. While PPAR α occupancy was not affected by the diet, GR and STAT5 co-occupancy increased near genes important for lipid and fatty acid metabolism.

High-Fat-Diet-Induced Reprogramming Is Driven by STAT5

To identify differential factors regulated by HFD or insulin resistance within the transcriptional complex shared by GR and STAT5, we performed ChIP-MS (GR ChIP coupled to mass spectrometry proteomics). Indeed, both STAT5 and the PPAR α heterodimer partner RXR were purified in the GR interactomes (Figures 5A and S5A). However, the proteomics experiments did not reveal other relevant candidates that might explain our observed HFD-induced increase in GR and STAT5 co-occupancy. For instance, chromatin remodelers, histone modifying enzymes, co-regulators, and transcription factors (such as SWI/SNF, CBP, HNF4 α , C/EBP, and NCOA5) were co-purified with GR, as expected (Fletcher et al., 2002; Oakley and Cidlowski, 2013), but these were similarly enriched under both conditions.

Focusing on GR and STAT5 themselves, hepatocyte-specific *GR* and *Stat5* knockout mice on HFD showed that STAT5 occupancy was not affected by the loss of GR, while GR binding at shared, gained sites was significantly reduced in *Stat5* mutants (Figures 5B, 5C, S5B, and S5C).

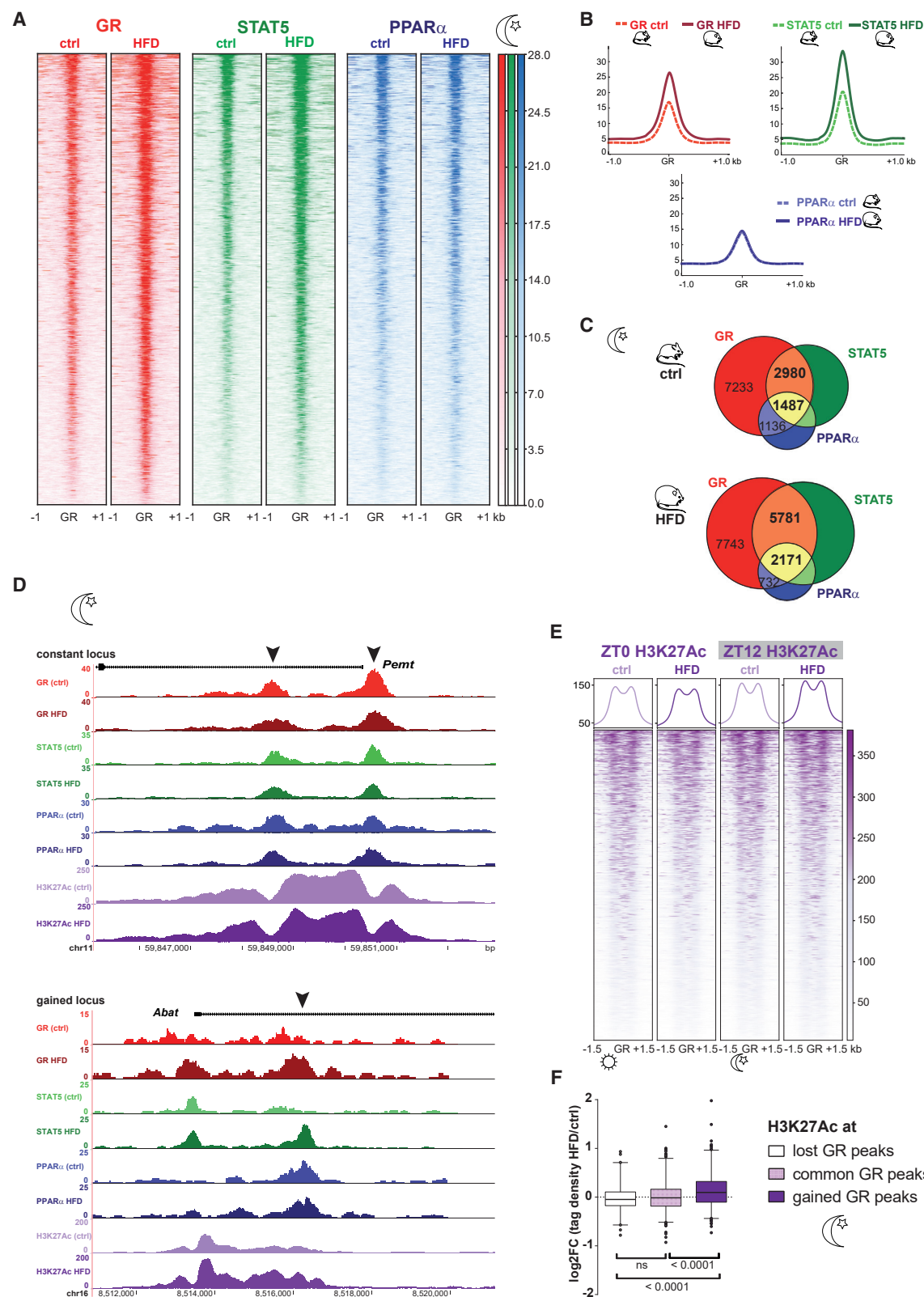
In conclusion, we saw that GR, PPAR α , and STAT5 co-occupied metabolic enhancers in HFD livers and that enhanced GR binding depended on the presence of STAT5. This observed increase in STAT5-GR co-occupancy might be due to altered JAK/STAT or GH signaling in insulin-resistant, obese animals.

Cistromic Reprogramming Affects Glucose and Triglyceride Metabolism

To test whether the HFD-induced binding events were functionally relevant, RNA-seq was performed for ZT0, ZT4, ZT8, ZT12,

Figure 3. GR Cistromes Are Reprogrammed by HFD

- Heatmap of GR genome-wide binding for ZT0–ZT20 in livers after 12 weeks of HFD. Each row shows the normalized unique tag counts for one GR ChIP peak of the union (sum of all reproducible peaks of the HFD dataset), ordered by signal strength.
- GR ChIP peak percent distribution over the indicated genomic regions for ZT0–ZT20 on HFD.
- Normalized distribution of GR ChIP-seq tag density in HFD and control cistromes for the six time points.
- Motif analyses of the 3,258 day and the 16,954 night-specific HFD GR ChIP-sequences show co-occurring hepatic transcription factors.
- Venn diagram comparing the GR ChIP peak overlap for the sum of all 3 night samples (ZT12, ZT16, and ZT20) from HFD and control livers. Genomic Regions Enrichment of Annotations Tool (GREAT) functional annotation is based on the nearest genes of the 9,345 additional HFD GR-binding sites.
- Enriched motifs in the GR ChIP peaks gained on HFD during the dark phase over the GR union used as background. Data presented is from two biological replicates per time point.
- Heatmap of transcripts associated with gained GR binding from (E) (9,354) and deregulated by HFD during the night (ZT12, ZT16, and ZT20). Pathway annotation for transcripts either up- or downregulated in HFD livers.



(legend on next page)

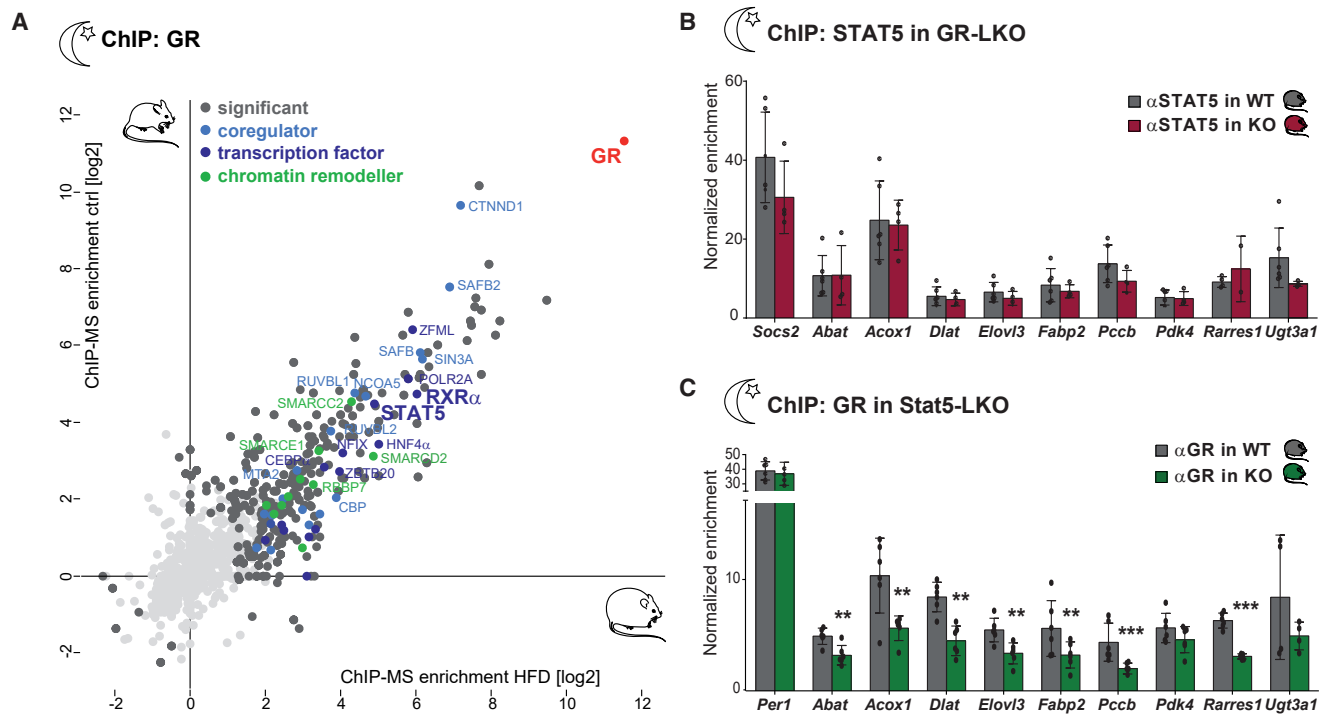


Figure 5. Cistromic Reprogramming by HFD Is Driven by STAT5 Occupancy

(A) GR interactomes (ChIP-MS) in HFD and control livers at ZT12. Enrichment (log2 fold change) of GR immunoprecipitation (IP) samples versus immunoglobulin G (IgG) (n = 3) was calculated for control and HFD diet samples (Fisher's exact test, false discovery rate [FDR] < 0.05, s0 = 1). (B) STAT5 ChIP-qPCR in GR-LKO (*Alb-Cre x GR^{fl/fl}*) and WT (*GR^{fl/fl}*) livers on HFD. The *Socs2* locus is a positive control for STAT5 binding that was not changed by HFD; the other loci showed HFD-induced gained GR-STAT5 co-occupancy by ChIP-seq. (C) GR ChIP-qPCR in STAT5a/b-LKO (*Alb-Cre x Stat5^{fl/fl}*) and WT (*Stat5^{fl/fl}*) livers on HFD. The *Per1* locus is a positive control for GR binding that was not changed by HFD; the other loci are the same as above. Enrichment is calculated over a negative locus. Values are shown as mean \pm SEM (n = 2–6 per group), **p < 0.01, ***p < 0.001 (two tailed t test).

ZT16, and ZT20 in hepatocyte-specific *GR* knockouts. Again, more genes were differentially expressed during the night on HFD, corresponding to pathways including lipid, fatty acid, amino acid, and carbohydrate metabolism (Figures 6A, S6A, and S6B). Loss of *GR* once more caused a transcriptional dampening of circadian amplitude across all time points, with a large proportion of direct *GR* targets losing oscillation on HFD (Figures 6B, S6C, and S6D).

Moreover, to directly test whether the HFD-induced binding events were functionally relevant, we determined the differential expression of those genes harboring a gained *GR* peak nearby,

specifically during the feeding phase (Figure 6C). Indeed, more than 400 gained targets were de-regulated in the absence of *GR*, with the upregulation of lipid and fatty acid metabolism being the most prominent. These *GR*-dependent changes occurred despite similar mRNA expression of the core clock machinery itself (except for *Per1*) (Figure S6D).

In accordance with our next-generation sequencing (NGS) profiles, *GR* mutants were prone to develop hepatic steatosis, which was exacerbated by HFD, and had lower blood glucose levels specifically during the night (Figures 6D–6G, S6E, and S6F). Strikingly, circulating triglycerides were lower only

Figure 4. GR, PPAR α , and STAT5 Signaling Pathways Intersect at Functional Enhancers

(A) Heatmap of GR, STAT5, and PPAR α genome-wide binding in control and HFD livers at ZT12. Each row shows the normalized unique ChIP-seq tag counts for GR, STAT5, and PPAR α centered on the GR peak positions and ordered by signal strength. (B) Normalized distribution of GR, STAT5, and PPAR α ChIP-seq tag density in control and HFD livers at ZT12 at sites occupied by GR. (C) Venn diagram of GR (12,836 and 16,427 peaks), STAT5 (8,815 and 14,216 peaks), and PPAR α (4,317 and 4,438 peaks) cistromes at ZT12 in control and HFD, respectively. (D) Representative examples of normalized GR, STAT5, PPAR α , and H3K27ac ChIP-seq tracks in both control and HFD at ZT12. Top: the *Permt* locus was not affected by diet. Bottom: the *Abat* locus gained GR-STAT5 co-occupancy together with increased H3K27ac on HFD. (E) ChIP-seq profiles for H3K27ac centered around GR peaks at ZT0 and ZT12 in HFD and control livers. Each row shows the normalized H3K27ac ChIP-seq tag counts ordered by signal strength. (F) Box plot (median, interquartile range, minimum, and maximum) of the log2 fold change between HFD and control tag density of H3K27ac ZT12 signal mapped to the “lost” (3,076), “common” (10,616), or “gained” (9,354) GR sites from Figure 3E. Only peaks near transcripts upregulated by HFD during the night were used. p values were determined using the Mann-Whitney test.

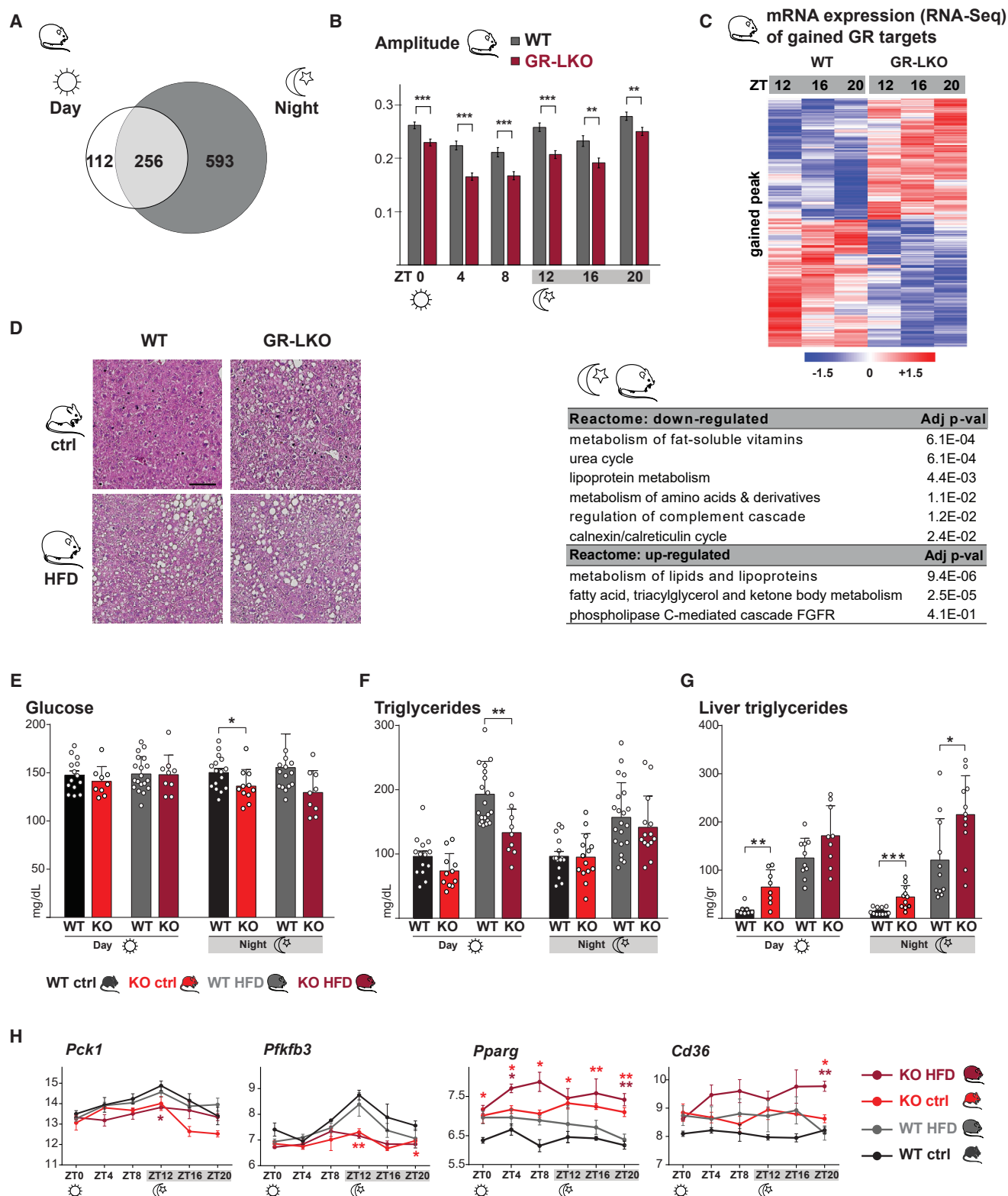


Figure 6. Liver-Specific GR Mutants Show Deregulation of Glucose and Triglyceride Metabolism

(A) Venn diagram showing number of differentially regulated genes in GR-LKO (*Alb-Cre* × *GR^{fl/fl}*) during the day (ZT0, ZT4, and ZT8) and night (ZT12, ZT16, and ZT20) after 12 weeks of HFD.

(legend continued on next page)

during the day, which was more evident on HFD, while liver triglycerides were significantly higher (Figures 6F and 6G). These physiological changes could be explained by the reduced expression of gluconeogenic genes like *Pck1* or *Pfkfb3* and by the increased expression of genes involved in lipid and fatty acid utilization and storage, such as *Cd36* and *PPAR γ* , in the absence of GR (Figure 6H). *PPAR γ* had previously been implicated in circadian remodeling by HFD, in accordance with these observations (Eckel-Mahan et al., 2013).

In sum, we found that GR alters temporal gene expression profiles by sustaining oscillations. We could functionally link these gene expression changes to nearby GR-binding events by using hepatocyte-specific GR mutants. Several hundreds of genes displayed *de novo* GR binding and GR dependence on HFD. We showed that the pathways targeted by GR are mainly regulating energy homeostasis and that they control circulating glucose and triglyceride levels distinctly during times of feeding and fasting.

Ligand-Independent Genomic Responses on HFD

To further demonstrate that this increase in DNA-bound GR was indeed due to nutritional or pathogenic effects directly on the chromatin level, we treated both HFD and control mice with a single dose of the exogenous GR ligand dexamethasone (Dex). Animals were injected at ZT0 (lowest endogenous GCs), and livers were processed for GR ChIP-seq 1 h later. As expected, Dex treatment led to a significant increase in GR ChIP signal intensity (compared to untreated mice at ZT0), presumably resulting from increased occupancy in response to ligand. Interestingly, in HFD mice, GR binding after Dex was enhanced compared to mice on control diet, resulting in a gain of signal strength (Figures 7A and 7B). Importantly, this confirms that we measured increased GR occupancy in the face of identical ligand levels.

Furthermore, when we harvested livers 4 h after Dex injection (at ZT4), we detected a diet-specific differential effect on mRNA expression in obese animals (Figure 7C). RNA-seq revealed several hundreds of deregulated transcripts that responded differently to GR ligand on HFD. These HFD-specific GC responses could be annotated to circadian rhythms, *PPAR α* signaling, and lipid and cholesterol metabolism (Figure 7D).

We performed analogous experiments at the peak of GC secretion, injecting mice at ZT12 and harvesting control and HFD livers for ChIP-seq and RNA-seq 1 and 4 h later, respectively. Once more, we confirmed the increased GR ChIP-seq signal in livers from HFD-fed mice, in spite of identical doses of

Dex (with two different antibodies; Figure S7A). However, we did not observe major diet-specific mRNA changes in the Dex response at ZT16, conceivably because GR ligand levels are already very high at night (Figure S7B).

Taken together, we observed an augmented response to exogenous GC treatment on HFD, with identical ligand doses resulting in increased chromatin occupancy of GR at both ZT0 and ZT12. Of note, this altered genomic GC action manifested as differential regulation of metabolic and clock-associated gene expression programs during the fasting period.

DISCUSSION

Rhythmic GR Binding Strengthens Transcriptional Clock Output in Mouse Livers

We find that GR binding has a distinct daily pattern closely mirroring ligand availability, with low endogenous GC levels leading to promoter proximal binding near housekeeping and gluconeogenic genes during the day. In contrast, the nightly GC surge results in GR binding to distant metabolic enhancers regulating lipid and amino acid metabolism only during the feeding phase. It appears that GR only reaches those distant enhancers at higher hormone concentrations, which in turn allows the control of these metabolic gene networks only when needed. This implies that GCs govern nutrient partitioning and substrate utilization during daily cycles of feeding/fasting.

Our NGS studies show that the majority of diurnally oscillating transcripts are direct GR targets. GR interacts with core clock factors to enlarge and stabilize the amplitude of downstream target genes. Apparently, GR synchronizes 24-h rhythms by integrating circadian clock loops with hormone release and by coordinating metabolic fuel shifts. GR reinforces the core BMAL1/CLOCK/PER/CRY and the ancillary REV-ERB/ROR loops and generates rhythmic outputs (Figure S2D). Our observations again emphasize the tight connection between mammalian circadian rhythms and metabolism.

The Nutritional State Modifies GC Action

Surprisingly, we find that HFD expands the GR cistrome, mainly during the feeding phase. This gain in GR ChIP signal was observed despite comparable endogenous corticosterone levels. Although there is a discrepancy in the literature with regard to GC levels in HFD-fed mice (Auvinen et al., 2012; Kohsaka et al., 2007), we did not measure any effect of the diet on the amount of circulating hormones in our cohort. That means that nutrition changes hormone responses at the genomic level and

(B) Amplitude distribution for ZT0–ZT20 in livers from GR-LKO compared to GR^{fl/fl} littermates (WT) on HFD. Values are represented as mean \pm SEM (n = 3 per group).

(C) Heatmap of deregulated transcripts in GR-LKO during the night (ZT12, 16, 20) associated with “gained” (9,354) GR peaks from Figure 3E. Pathway annotation was performed for transcripts either up- or downregulated in GR-LKO livers.

(D) H&E staining of livers from GR-LKO mice and littermate controls after 12 weeks of high-fat or control diet. One representative section from n = 3 biological replicates is shown (scale bar, 100 μ M).

(E–G) Blood glucose (E), serum triglycerides (F), and liver triglycerides (G) from GR-LKO mice and littermate controls during the day (ZT0, ZT4, and ZT8) or night (ZT12, ZT16, and ZT20) on high-fat or control diet. Values are represented as mean \pm SD (n = 8–20 per group).

(H) RNA-seq data (normalized read counts, Rlog) for deregulated gluconeogenic (*Pck1* and *Pfkfb3*) and lipid metabolism (*Ppar γ* and *CD36*) transcripts in GR-LKO mice and controls fed with high-fat or control diet.

Values are represented as mean \pm SEM (n = 3 per group); *p < 0.05, **p < 0.01, ***p < 0.001 (two tailed t test).



(B) Normalized distribution of GR ChIP-seq tag density, corresponding to (A).

(D) Pathway annotation of transcripts down- (n = 374) and upregulated (n = 608) by Dex treatment in HFD livers compared to controls.

Our observations agree with published studies showing that HFD alters the epigenome and consequently enhancer activity, for example by increasing H3K27 acetylation, DNaseI hypersensitivity, and enhancer RNA (eRNA) oscillations (Guan et al., 2018; Leung et al., 2016; Siersbæk et al., 2017; Soltis et al., 2017). Therefore, the enhanced GR occupancy might possibly benefit from increased chromatin accessibility.

Our studies identified PPAR α and STAT5 as interacting with GR in the liver, but we cannot exclude the possibility that other nuclear receptors or transcription factors may also be cross-talking with GR. We focused our analysis on PPAR α , for it is a well-known master regulator of hepatic lipid metabolism and, like GR, a fasting-induced receptor (Goldstein et al., 2017; Kersten et al., 1999). However, it is possible that the DR1 motif we identified is bound by other RXR-heterodimerizing nuclear receptors such as other PPARs, FXR, or LXRs.

The enrichment of both the STAT5 motif in the GR peaks, as well as the protein itself in the GR interactome, correlates well with the dramatic increase of STAT5 occupancy in HFD livers. Using liver-specific mutants, we show that the enhanced GR binding is indeed dependent on STAT5. One possible explanation might be differential post-translational

modifications on HFD or rather insulin resistance. We could not detect any difference in STAT5 Y694 phosphorylation status, the site that is essential for DNA binding and transcriptional activation (Gouilleux et al., 1994), in HFD versus control liver extracts (data not shown). Nonetheless, we cannot rule out the presence of other modifications affecting STAT5 activity. At this point, we do not know whether this augmented GC-JAK-STAT response results from altered cytokine or GH/IGF1/insulin signaling in obese mice or from changes in the chromatin landscape induced by nutritional adaptation.

Hepatic GR Controls Glucose and Triglyceride Metabolism

Finally, we found that the gene programs controlled by GR's temporal occupancy are essential for glucose, lipid, and fatty acid metabolism during daily alternations between feeding and fasting. Hepatocyte-specific GR knockouts have lower levels of circulating glucose specifically at night and lower serum triglycerides during the day. Concomitantly, GR mutants are prone to develop hepatic steatosis. GR \times Stat5 liver-specific double-mutant mice progress to hepatocellular carcinoma, which might link the GR-STAT5 signature to the development of liver cancer and disease pathology (Mueller et al., 2011).

Altogether, our findings emphasize the key role GR plays for the temporal synchronization of metabolic rhythms in the liver and highlight its importance during the progression of metabolic disease.

STAR★METHODS

Detailed methods are provided in the online version of this paper and include the following:

- KEY RESOURCES TABLE
- LEAD CONTACT AND MATERIALS AVAILABILITY
- METHOD DETAILS
 - Animal Experiments
 - ELISA
 - Triglyceride assay
 - Histology
 - RNA isolation and sequencing
 - Chromatin Immunoprecipitation (ChIP)
 - ChIP-DNA Sequencing
 - ChIP-qPCR
 - Total protein extraction
 - Nuclear protein extraction
 - Western blot
 - ChIP-MS
- QUANTIFICATION AND STATISTICAL ANALYSIS
- BIOINFORMATICS (SEE FIGURE S1G)
 - ChIP-Seq
 - RNA-Seq
 - ChIP-MS
- DATA AND CODE AVAILABILITY

SUPPLEMENTAL INFORMATION

Supplemental Information can be found online at <https://doi.org/10.1016/j.molcel.2019.10.007>.

ACKNOWLEDGMENTS

We sincerely thank the NGS Core Facility (HMGU), with S. Lösecke, T. Schwarzmayr, T. Strom, and E. Graf, and the MDC genomics core, with N. Hübner, for their contribution. We are grateful to S. Schön, V. Sportelli, K. Beresowski, T. Horn, B. Haderlein, M. Mataboni, H.K. Jambor, T. Müller, K. Biniossek, I. Guderian, and S. Regn for assistance. We thank the Tuckermann Lab (Ulm) for GR floxed mice and the Moriggl Lab (Vienna) for STAT5 floxed alleles. This work was supported by funding from the SNSF (P2LAP3_164906) to C.J., the NIH (R01 DK108987) to G.D.B., the NCI NIH (CA154887) and the German Science Alliance on Precision Medicine and Cancer Prevention to F.V.F., and the DFG (UH 275/1-1) and ERC (ERC-2014-StG 638573 SILENCE) to N.H.U.

AUTHOR CONTRIBUTIONS

Conceptualization, F.Q. and N.H.U.; Investigation, F.Q., M.W., K.M., K.A.D., C.J., and G.D.B.; Formal Analysis, A.A.M., K.B., F.V.F., J.H., and M.H.; Methodology, F.Q., A.A.M., and G.D.B.; Validation, F.Q.; Writing, F.Q. and N.H.U.; Funding Acquisition, N.H.U., C.J., and G.D.B.; Supervision, N.H.U.

DECLARATION OF INTERESTS

The authors declare no competing interests.

Received: February 8, 2018

Revised: August 2, 2019

Accepted: October 7, 2019

Published: November 6, 2019

REFERENCES

- Allhoff, M., Seré, K., F. Pires, J., Zenke, M., and G Costa, I. (2016). Differential peak calling of ChIP-seq signals with replicates with THOR. *Nucleic Acids Res.* 44, e153.
- Auvinen, H.E., Romijn, J.A., Biermasz, N.R., Pijl, H., Havekes, L.M., Smit, J.W., Rensen, P.C., and Pereira, A.M. (2012). The effects of high fat diet on the basal activity of the hypothalamus-pituitary-adrenal axis in mice. *J. Endocrinol.* 214, 191–197.
- Baik, M., Yu, J.H., and Hennighausen, L. (2011). Growth hormone-STAT5 regulation of growth, hepatocellular carcinoma, and liver metabolism. *Ann. N Y Acad. Sci.* 1229, 29–37.
- Balsalobre, A., Brown, S.A., Marcacci, L., Tronche, F., Kellendonk, C., Reichardt, H.M., Schütz, G., and Schibler, U. (2000). Resetting of circadian time in peripheral tissues by glucocorticoid signaling. *Science* 289, 2344–2347.
- Barclay, J.L., Husse, J., Bode, B., Naujokat, N., Meyer-Kovac, J., Schmid, S.M., Lehnert, H., and Oster, H. (2012). Circadian desynchrony promotes metabolic disruption in a mouse model of shiftwork. *PLoS ONE* 7, e37150.
- Barnett, D.W., Garrison, E.K., Quinlan, A.R., Strömberg, M.P., and Marth, G.T. (2011). BamTools: a C++ API and toolkit for analyzing and managing BAM files. *Bioinformatics* 27, 1691–1692.
- Bass, J. (2016). Circadian mechanisms in bioenergetics and cell metabolism. In *A Time for Metabolism and Hormones*, P. Sassone-Corsi and Y. Christen, eds. (Springer, Cham), pp. 25–32.
- Bookout, A.L., Jeong, Y., Downes, M., Yu, R.T., Evans, R.M., and Mangelsdorf, D.J. (2006). Anatomical profiling of nuclear receptor expression reveals a hierarchical transcriptional network. *Cell* 126, 789–799.
- Chen, L., and Yang, G. (2014). PPARs integrate the mammalian clock and energy metabolism. *PPAR Res.* 2014, 653017.

- Cho, H., Zhao, X., Hatori, M., Yu, R.T., Barish, G.D., Lam, M.T., Chong, L.W., DiTacchio, L., Atkins, A.R., Glass, C.K., et al. (2012). Regulation of circadian behaviour and metabolism by REV-ERB- α and REV-ERB- β . *Nature* **485**, 123–127.
- Cox, J., Hein, M.Y., Luber, C.A., Paron, I., Nagaraj, N., and Mann, M. (2014). Accurate proteome-wide label-free quantification by delayed normalization and maximal peptide ratio extraction, termed MaxLFQ. *Mol. Cell Proteomics* **13**, 2513–2526.
- Cui, Y., Riedlinger, G., Miyoshi, K., Tang, W., Li, C., Deng, C.X., Robinson, G.W., and Hennighausen, L. (2004). Inactivation of Stat5 in mouse mammary epithelium during pregnancy reveals distinct functions in cell proliferation, survival, and differentiation. *Mol. Cell. Biol.* **24**, 8037–8047.
- Damiola, F., Le Minh, N., Preitner, N., Kornmann, B., Fleury-Olela, F., and Schibler, U. (2000). Restricted feeding uncouples circadian oscillators in peripheral tissues from the central pacemaker in the suprachiasmatic nucleus. *Genes Dev.* **14**, 2950–2961.
- Dobin, A., Davis, C.A., Schlesinger, F., Drenkow, J., Zaleski, C., Jha, S., Batut, P., Chaisson, M., and Gingeras, T.R. (2013). STAR: ultrafast universal RNA-seq aligner. *Bioinformatics* **29**, 15–21.
- Eckel-Mahan, K., and Sassone-Corsi, P. (2013). Metabolism and the circadian clock converge. *Physiol. Rev.* **93**, 107–135.
- Eckel-Mahan, K.L., Patel, V.R., de Mateo, S., Orozco-Solis, R., Ceglia, N.J., Sahar, S., Dilag-Penilla, S.A., Dyar, K.A., Baldi, P., and Sassone-Corsi, P. (2013). Reprogramming of the circadian clock by nutritional challenge. *Cell* **155**, 1464–1478.
- Engblom, D., Kornfeld, J.W., Schwake, L., Tronche, F., Reimann, A., Beug, H., Hennighausen, L., Moriggl, R., and Schütz, G. (2007). Direct glucocorticoid receptor-Stat5 interaction in hepatocytes controls body size and maturation-related gene expression. *Genes Dev.* **21**, 1157–1162.
- Fang, B., Everett, L.J., Jager, J., Briggs, E., Armour, S.M., Feng, D., Roy, A., Gerhart-Hines, Z., Sun, Z., and Lazar, M.A. (2014). Circadian enhancers coordinate multiple phases of rhythmic gene transcription in vivo. *Cell* **159**, 1140–1152.
- Feng, J., Liu, T., and Zhang, Y. (2011). Using MACS to identify peaks from ChIP-Seq data. *Curr. Protoc. Bioinformatics Chapter 2*. Unit 2.14.
- Fletcher, T.M., Xiao, N., Mautino, G., Baumann, C.T., Wolford, R., Warren, B.S., and Hager, G.L. (2002). ATP-dependent mobilization of the glucocorticoid receptor during chromatin remodeling. *Mol. Cell. Biol.* **22**, 3255–3263.
- Goldstein, I., Baek, S., Presman, D.M., Paakinaho, V., Swinstead, E.E., and Hager, G.L. (2017). Transcription factor assisted loading and enhancer dynamics dictate the hepatic fasting response. *Genome Res.* **27**, 427–439.
- Gouilleux, F., Wakao, H., Mundt, M., and Groner, B. (1994). Prolactin induces phosphorylation of Tyr694 of Stat5 (MGF), a prerequisite for DNA binding and induction of transcription. *EMBO J.* **13**, 4361–4369.
- Greulich, F., Hemmer, M.C., Rollins, D.A., Rogatsky, I., and Uhlenhaut, N.H. (2016). There goes the neighborhood: assembly of transcriptional complexes during the regulation of metabolism and inflammation by the glucocorticoid receptor. *Steroids* **114**, 7–15.
- Guan, D., Xiong, Y., Borck, P.C., Jang, C., Doulias, P.T., Papazyan, R., Fang, B., Jiang, C., Zhang, Y., Briggs, E.R., et al. (2018). Diet-induced circadian enhancer remodeling synchronizes opposing hepatic lipid metabolic processes. *Cell* **174**, 831–842.e812.
- Hein, M.Y., Hubner, N.C., Poser, I., Cox, J., Nagaraj, N., Toyoda, Y., Gak, I.A., Weisswange, I., Mansfeld, J., Buchholz, F., et al. (2015). A human interactome in three quantitative dimensions organized by stoichiometries and abundances. *Cell* **163**, 712–723.
- Heinz, S., Benner, C., Spann, N., Bertolino, E., Lin, Y.C., Laslo, P., Cheng, J.X., Murre, C., Singh, H., and Glass, C.K. (2010). Simple combinations of lineage-determining transcription factors prime cis-regulatory elements required for macrophage and B cell identities. *Mol. Cell* **38**, 576–589.
- Hughes, M.E., Hogenesch, J.B., and Kornacker, K. (2010). JTK_CYCLE: an efficient nonparametric algorithm for detecting rhythmic components in genome-scale data sets. *J. Biol. Rhythms* **25**, 372–380.
- Kersten, S., Seydoux, J., Peters, J.M., Gonzalez, F.J., Desvergne, B., and Wahli, W. (1999). Peroxisome proliferator-activated receptor alpha mediates the adaptive response to fasting. *J. Clin. Invest.* **103**, 1489–1498.
- Kohsaka, A., Laposky, A.D., Ramsey, K.M., Estrada, C., Joshi, C., Kobayashi, Y., Turek, F.W., and Bass, J. (2007). High-fat diet disrupts behavioral and molecular circadian rhythms in mice. *Cell Metab.* **6**, 414–421.
- Koike, N., Yoo, S.H., Huang, H.C., Kumar, V., Lee, C., Kim, T.K., and Takahashi, J.S. (2012). Transcriptional architecture and chromatin landscape of the core circadian clock in mammals. *Science* **338**, 349–354.
- Kuleshov, M.V., Jones, M.R., Rouillard, A.D., Fernandez, N.F., Duan, Q., Wang, Z., Koplev, S., Jenkins, S.L., Jagodnik, K.M., Lachmann, A., et al. (2016). Enrichr: a comprehensive gene set enrichment analysis web server 2016 update. *Nucleic Acids Res.* **44** (W1), W90–W97.
- Lamia, A., Papp, S.J., Yu, R.T., Barish, G.D., Uhlenhaut, N.H., Jonker, J.W., Downes, M., and Evans, R.M. (2011). Cryptochromes mediate rhythmic repression of the glucocorticoid receptor. *Nature* **480**, 552–556.
- Leung, A., Trac, C., Du, J., Natarajan, R., and Schones, D.E. (2016). Persistent chromatin modifications induced by high fat diet. *J. Biol. Chem.* **291**, 10446–10455.
- Li, H., and Durbin, R. (2010). Fast and accurate long-read alignment with Burrows-Wheeler transform. *Bioinformatics* **26**, 589–595.
- Li, H., Handsaker, B., Wysoker, A., Fennell, T., Ruan, J., Homer, N., Marth, G., Abecasis, G., and Durbin, R.; 1000 Genome Project Data Processing Subgroup (2009). The Sequence Alignment/Map format and SAMtools. *Bioinformatics* **25**, 2078–2079.
- Liao, Y., Smyth, G.K., and Shi, W. (2014). featureCounts: an efficient general purpose program for assigning sequence reads to genomic features. *Bioinformatics* **30**, 923–930.
- Lim, H.W., Uhlenhaut, N.H., Rauch, A., Weiner, J., Hübner, S., Hübner, N., Won, K.J., Lazar, M.A., Tuckermann, J., and Steger, D.J. (2015). Genomic redistribution of GR monomers and dimers mediates transcriptional response to exogenous glucocorticoid in vivo. *Genome Res.* **25**, 836–844.
- Love, M.I., Huber, W., and Anders, S. (2014). Moderated estimation of fold change and dispersion for RNA-seq data with DESeq2. *Genome Biol.* **15**, 550.
- Marcheva, B., Ramsey, K.M., Peek, C.B., Affinati, A., Maury, E., and Bass, J. (2013). Circadian clocks and metabolism. *Handb. Exp. Pharmacol.* **217**, 127–155.
- McLean, C.Y., Bristor, D., Hiller, M., Clarke, S.L., Schaar, B.T., Lowe, C.B., Wenger, A.M., and Bejerano, G. (2010). GREAT improves functional interpretation of cis-regulatory regions. *Nat Biotechnol* **28**, 495–501.
- Mir, A.A., Dyar, K.A., Greulich, F., Quagliarini, F., Jouffe, C., Hubert, M.J., Hemmer, M.C., and Uhlenhaut, N.H. (2019). In vivo ChIP-Seq of nuclear receptors: a rough guide to transform frozen tissues into high-confidence genome-wide binding profiles. *Methods Mol. Biol.* **1966**, 39–70.
- Mueller, K.M., Kornfeld, J.W., Friedbichler, K., Blaas, L., Egger, G., Esterbauer, H., Hasselblatt, P., Schleder, M., Haindl, S., Wagner, K.U., et al. (2011). Impairment of hepatic growth hormone and glucocorticoid receptor signaling causes steatosis and hepatocellular carcinoma in mice. *Hepatology* **54**, 1398–1409.
- Mueller, K.M., Themanns, M., Friedbichler, K., Kornfeld, J.W., Esterbauer, H., Tuckermann, J.P., and Moriggl, R. (2012). Hepatic growth hormone and glucocorticoid receptor signaling in body growth, steatosis and metabolic liver cancer development. *Mol. Cell. Endocrinol.* **367**, 1–11.
- Nader, N., Chrousos, G.P., and Kino, T. (2009). Circadian rhythm transcription factor CLOCK regulates the transcriptional activity of the glucocorticoid receptor by acetylating its hinge region lysine cluster: potential physiological implications. *FASEB J.* **23**, 1572–1583.
- Oakley, R.H., and Cidlowski, J.A. (2013). The biology of the glucocorticoid receptor: new signaling mechanisms in health and disease. *J. Allergy Clin. Immunol.* **132**, 1033–1044.
- Oishi, K., Amagai, N., Shirai, H., Kadota, K., Ohkura, N., and Ishida, N. (2005). Genome-wide expression analysis reveals 100 adrenal gland-dependent circadian genes in the mouse liver. *DNA Res.* **12**, 191–202.

- Opferk, C., Tronche, F., Kellendonk, C., Kohlmüller, D., Schulze, A., Schmid, W., and Schutz, G. (2004). Inactivation of the glucocorticoid receptor in hepatocytes leads to fasting hypoglycemia and ameliorates hyperglycemia in streptozotocin-induced diabetes mellitus. *Mol. Endocrinol.* **18**, 1346–1353.
- Panda, S. (2016). Circadian physiology of metabolism. *Science* **354**, 1008–1015.
- Patel, R., Williams-Dautovich, J., and Cummins, C.L. (2014). Minireview: new molecular mediators of glucocorticoid receptor activity in metabolic tissues. *Mol. Endocrinol.* **28**, 999–1011.
- Pawlak, M., Lefebvre, P., and Staels, B. (2015). Molecular mechanism of PPAR α action and its impact on lipid metabolism, inflammation and fibrosis in non-alcoholic fatty liver disease. *J. Hepatol.* **62**, 720–733.
- Preidis, G.A., Kim, K.H., and Moore, D.D. (2017). Nutrient-sensing nuclear receptors PPAR α and FXR control liver energy balance. *J. Clin. Invest.* **127**, 1193–1201.
- Quinlan, A.R. (2014). BEDTools: the Swiss-Army tool for genome feature analysis. *Curr. Protoc. Bioinformatics* **47**, 11.12.1–34.
- Reddy, A.B., Maywood, E.S., Karp, N.A., King, V.M., Inoue, Y., Gonzalez, F.J., Lilley, K.S., Kyriacou, C.P., and Hastings, M.H. (2007). Glucocorticoid signaling synchronizes the liver circadian transcriptome. *Hepatology* **45**, 1478–1488.
- Scheltema, R.A., Hauschild, J.P., Lange, O., Hornburg, D., Denisov, E., Damoc, E., Kuehn, A., Makarov, A., and Mann, M. (2014). The Q Exactive HF, a Benchtop mass spectrometer with a pre-filter, high-performance quadrupole and an ultra-high-field Orbitrap analyzer. *Mol. Cell Proteomics* **13**, 3698–3708.
- Siersbæk, M., Varticovski, L., Yang, S., Baek, S., Nielsen, R., Mandrup, S., Hager, G.L., Chung, J.H., and Grøntved, L. (2017). High fat diet-induced changes of mouse hepatic transcription and enhancer activity can be reversed by subsequent weight loss. *Sci. Rep.* **7**, 40220.
- So, A.Y., Bernal, T.U., Pillsbury, M.L., Yamamoto, K.R., and Feldman, B.J. (2009). Glucocorticoid regulation of the circadian clock modulates glucose homeostasis. *Proc. Natl. Acad. Sci. USA* **106**, 17582–17587.
- Soltis, A.R., Motola, S., Vernia, S., Ng, C.W., Kennedy, N.J., Dalin, S., Matthews, B.J., Davis, R.J., and Fraenkel, E. (2017). Hyper- and hypo- nutrition studies of the hepatic transcriptome and epigenome suggest that PPAR α regulates anaerobic glycolysis. *Sci. Rep.* **7**, 174.
- Spiegel, K., Tasali, E., Leproult, R., and Van Cauter, E. (2009). Effects of poor and short sleep on glucose metabolism and obesity risk. *Nat. Rev. Endocrinol.* **5**, 253–261.
- Spiga, F., Walker, J.J., Terry, J.R., and Lightman, S.L. (2014). HPA axis-rhythms. *Compr. Physiol.* **4**, 1273–1298.
- Takahashi, J.S. (2017). Transcriptional architecture of the mammalian circadian clock. *Nat. Rev. Genet.* **18**, 164–179.
- Torra, I.P., Tsubulsky, V., Delaunay, F., Saladin, R., Laudet, V., Fruchart, J.C., Kosykh, V., and Staels, B. (2000). Circadian and glucocorticoid regulation of Rev-erb α expression in liver. *Endocrinology* **141**, 3799–3806.
- Uhlenhaut, N.H., Barish, G.D., Yu, R.T., Downes, M., Karunasiri, M., Liddle, C., Schwalie, P., Hubner, N., and Evans, R.M. (2013). Insights into negative regulation by the glucocorticoid receptor from genome-wide profiling of inflammatory cistromes. *Mol. Cell* **49**, 158–171.
- Wilson, S., Qi, J., and Filipp, F.V. (2016). Refinement of the androgen response element based on ChIP-Seq in androgen-insensitive and androgen-responsive prostate cancer cell lines. *Sci. Rep.* **6**, 32611.
- Wilson, S., Fan, L., Sahgal, N., Qi, J., and Filipp, F.V. (2017). The histone demethylase KDM3A regulates the transcriptional program of the androgen receptor in prostate cancer cells. *Oncotarget* **8**, 30328–30343.
- Wu, G., Anafi, R.C., Hughes, M.E., Komacker, K., and Hogenesch, J.B. (2016). MetaCycle: an integrated R package to evaluate periodicity in large scale data. *Bioinformatics* **32**, 3351–3353.
- Yamamoto, T., Nakahata, Y., Tanaka, M., Yoshida, M., Soma, H., Shinohara, K., Yasuda, A., Mamine, T., and Takumi, T. (2005). Acute physical stress elevates mouse period1 mRNA expression in mouse peripheral tissues via a glucocorticoid-responsive element. *J. Biol. Chem.* **280**, 42036–42043.
- Yang, X., Downes, M., Yu, R.T., Bookout, A.L., He, W., Straume, M., Mangelsdorf, D.J., and Evans, R.M. (2006). Nuclear receptor expression links the circadian clock to metabolism. *Cell* **126**, 801–810.
- Zhang, Y., Fang, B., Emmett, M.J., Damle, M., Sun, Z., Feng, D., Armour, S.M., Remsberg, J.R., Jager, J., Soccio, R.E., et al. (2015). GENE REGULATION. Discrete functions of nuclear receptor Rev-erb α couple metabolism to the clock. *Science* **348**, 1488–1492.

STAR★METHODS

KEY RESOURCES TABLE

REAGENT or RESOURCE	SOURCE	IDENTIFIER
Antibodies		
Anti-GR (M-20)	Santa Cruz Biotech	Cat#sc-1004; RRID:AB_2155786
Anti-GR	ProteinTech Group	Cat#24050-1-AP; RRID:AB_2813890
Anti-GR (G-5)	Santa Cruz Biotech	Cat#sc-393232; RRID:AB_2687823
Anti-Stat5 a/b	RD System	Cat#AF2168; RRID:AB_355174
Anti-Stat5 a (pY694)	Cell Signaling Technology	Cat#9351; RRID: AB_331593
Anti-Stat5 (D2O6Y)	Cell Signaling Technology	Cat#94205; RRID:AB_2737403
Anti-Stat5 a/b	Abcam	Cat#ab194898
Anti-Cry1	Abcam	Cat# ab104736; RRID:AB_10710308
Anti-Cry2	Katja Lamia (Scripps)	N/A
Anti-PPARalpha (H-98)	Santa Cruz Biotech	Cat#sc-9000X; RRID:AB_2165737
Anti-AKT (pS473)	Santa Cruz Biotech	Cat#sc-7985; RRID:AB_667741
Anti-AKT	Cell Signaling Technology	Cat#4685; RRID:AB_2225340
Anti-H3k27ac	Abcam	Cat#ab4729; RRID: AB_2118291
Anti-rabbit IgG	Santa Cruz Biotech	Cat# sc-2317; RRID:AB_641182
Anti-mouse IgG	Bio-Rad	Cat# 170-6516; RRID:AB_11125547
Anti-guinea pig IgG	Santa Cruz Biotech	Cat# sc-2438; RRID:AB_650492
Chemicals, Peptides, and Recombinant Proteins		
Dynabeads M-280 Sheep Anti-Rabbit IgG	Life Technologies	11204D
Sepharose Protein A/G	Rockland	PAG50-00-0002
QIAzol Lysis Reagent (200ml)	QIAGEN	79306
DSG Crosslinker	Proteochem	C1104
16% Formaldehyde (w/v), Methanol-free	Thermo Scientific	28906
Gel Cassettes, Pippin Prep, dye-free	Sage Science	CDF2010
Power Sybr Green Mastermix	Thermo Scientific	4367659
DEXAMETHASONE-WATER SOLUBLE	Sigma	D2915
4-12% Bis-Tris SDS-PAGE gel	Life Technologies	NP0323BOX
Critical Commercial Assays		
Kapa Hyper Prep	Roche	7962363001
Lib Quant Illumina Rox Low	Roche	7960336001
Agilent RNA 6000 Nano Kit	Agilent Technologies	5067-1511
High Sensitivity DNA Kit	Agilent Technologies	5067-4626
Corticosterone Enzyme Immunoassay Kit	Arbor assay	K014-H1
LabAssay Triglyceride	Wako	290-63701
Deposited Data		
ChIP-Seq	GEO project	GSE108690
RNA-Seq	GEO project	GEO: GSE108690
ChIP-MS	PRIDE archive (EBI)	PRIDE: PXD014030
Experimental Models: Organisms/Strains		
C57BL/6J	Janvier	N/A
Albumin-Cre	Jackson Lab	N/A
GR flox/flox	Opherk et al., 2004	N/A
Stat5a/b flox/flox	Cui et al., 2004	N/A

(Continued on next page)

Continued

REAGENT or RESOURCE	SOURCE	IDENTIFIER
Oligonucleotides		
Table S2	N/A	N/A
Software and Algorithms		
Bwgenome read mapper	Welcome Trust Sanger Institute	Version 7.12
STAR RNA-Seq read mapper	Cold Spring Harbor Laboratory	Version 2.4.2a
DESeq2	Genome Biology Unit, European Molecular Biology Laboratory	Version 1.23.10
JTK cycle	Yale School of Medicine	MetaCycle version 1.2.0
samtools	Welcome Trust Sanger Institute	Version 1.3.1
HOMER	UCSD	Version 4.8
Bamtools	Boston College	Version 2.4.0
Deeptools	Max Planck Institute of Immunobiology and Epigenetics	Version 2.2.4
UCSC toolkit	University of California Santa Cruz	macOSX.x86_64
Bedtools	University of Virginia	Version 2.25.0
Max Quant	Max Plank Institute of Biochemistry	Version 1.5.3.29
Perseus	Max Plank Institute of Biochemistry	Version 1.5.3.0
Other		
58 kcal% fat w/sucrose	Research Diets	D12331
11 kcal% fatw/sucrose	Research Diets	D12329

LEAD CONTACT AND MATERIALS AVAILABILITY

Further information and requests for resources and reagents should be directed to and will be fulfilled by the Lead Contact, Henriette Uhlenhaut (henriette.uhlenhaut@helmholtz-muenchen.de).

This study did not generate new unique reagents.

METHOD DETAILS

Animal Experiments

Male C57BL/6J mice were housed in a controlled environment (12h light/12h dark daily cycle, ~23°C) and fed either control diet (11 kcal% fat w/sucrose, Research Diets D12329) or High Fat Diet (58 kcal% fat w/sucrose, Research Diets D12331) for 12 weeks. At 18 weeks of age, mice were sacrificed by cervical dislocation, and livers plus blood were collected at the indicated 4 h intervals. Dexamethasone (Sigma, D2915) was administered at ZT0 and at ZT12 as a single i.p. injection of 10 mg/kg after 12 weeks of high fat or control diet. Mice were sacrificed by cervical dislocation 1 h and 4 h later. Hepatocyte-specific *Alb-Cre x GR^{fl}/flox* (Opher et al., 2004) and *Alb-Cre x Stat5^{flox}/flox* mice (Cui et al., 2004) and controls were placed on High Fat Diet or control diet for 12 weeks. Livers were collected after cervical dislocation. Glucose tolerance tests (GTT) were performed in mice fasted overnight. Glucose (20% D-glucose; Sigma Aldrich) was injected i.p. at 1.5 g/kg and blood glucose levels were determined using a glucometer (AccuCheck Aviva, Roche Diagnostics).

Mouse experiments were performed according to the rules and guidelines established by the Institutional Animal Committee at Helmholtz Center Munich. Ethical approval was received from the local animal welfare authority (District government of upper Bavaria ROB-55.2-2532.Vet_02-14-33 and AZ_55.2-1-54-2532-158-14).

ELISA

Serum corticosterone was assayed by an enzyme immunoassay kit from Arbor Assays (K014-H1) according to manufacturer's instructions.

Triglyceride assay

For triglyceride measurements, liver tissue was first digested in ethanol / 30% KOH (2:1, v/v) at 60°C. Digested samples were mixed with 1M MgCl₂ at a ratio of 1.08:1 (volume) and incubated on ice for 10min followed by centrifugation. Supernatants and serum samples were measured by colorimetric assay (#290-63701, Wako Chemicals) following the company's instructions.

Histology

For H&E staining, 6 μ m PFA-fixed liver paraffin sections were treated with hematoxylin and eosin Y (#GHS332, Sigma Aldrich) using standard procedures. Brightfield microscopy was performed with a Keyence BZ-9000 microscope at a 10X magnification.

RNA isolation and sequencing

Total RNA was isolated from 50mg of liver using QIAzol (QIAGEN). Quality of the RNA was assayed using the Agilent RNA 6000 Nano Kit in a 2100 Bioanalyzer (Agilent). Libraries were prepped from 1 μ g total RNA with the Illumina TruSeq RNA library prep kit v2 chemistry in an automated system (Agilent Bravo liquid handling platform). Libraries were run on a HighSeq4000 sequencer (Illumina).

Chromatin Immunoprecipitation (ChIP)

ChIP was performed as previously described (Uhlenhaut et al., 2013; Mir et al., 2019). Briefly, 200mg of frozen liver were minced and Dounce homogenized in 0.7mg/mL DSG crosslinker (Proteochem) and 1% formaldehyde (Thermo Fisher Scientific). Nuclei were isolated and chromatin sonicated to a 0.1–1kb size using a Diagenode Bioruptor. Sheared chromatin was then immunoprecipitated with α -GR antibody (Santa Cruz, sc-1004X; Proteintech, 24050-1-AP), α -PPAR α antibody (Santa Cruz, sc-9000), α -STAT5a/b (RD System, AF2168; Cell Signaling, 94205; Abcam, ab194898), α -STAT5a/b (pY694/Y699) (Cell Signaling, 9351) or α -H3K27ac (Abcam, ab4729), and DNA was isolated with MinElute PCR Purification Kits (QIAGEN). DNA concentration was determined by using a QUBIT dsDNA HS kit (Thermo Fisher Scientific).

ChIP-DNA Sequencing

Libraries from ChIP and input DNA were prepared with the KAPA Hyperprep Kit (Kapa Biosystems, KK8504). Illumina compatible adapters were synthesized by IDT (Integrated DNA Technologies) and used at a final concentration of 68nM. Adaptor-ligated libraries were size selected (360–610bp) in a Pippin Gel station (Sage Science) using 2% dye free gels (Sage Science, CDF2010). Library concentrations were estimated by RT-PCR with the KAPA Library Quantification Kit (Kapa Biosystems, KK4873). Quality of the libraries was evaluated with the Agilent High Sensitivity DNA Kit in a 2100 Bioanalyzer (Agilent).

ChIP-qPCR

DNA was quantified by use of Power SYBR Green Master Mix (Life Technologies) in a ViiA 7 Real-Time PCR System (Thermo Fischer Scientific). Primers are listed in Table S2.

Total protein extraction

50mg of liver tissue were homogenized in RIPA buffer (150mM NaCl, 1% NP-40, 0.5% sodium deoxycholate, 0.1% SDS, 50mM Tris pH 8.0) supplemented with protease and phosphatase inhibitors.

Nuclear protein extraction

100mg liver tissue were homogenized in buffer containing 10mM HEPES-KOH pH 7.9, 1.5mM MgCl₂, 10mM KCl, 0.5mM DTT, 0.15% NP40 with protease and phosphatase inhibitors. After centrifugation, pellets were washed with PBS and nuclei were lysed in 2 vol buffer (10mM HEPES-KOH pH 7.9, 1.5mM MgCl₂, 10mM KCl, 0.5mM DTT, 0.1% NP40, 20% glycerol, with protease and phosphatase inhibitors) during 1 h incubation (rotating). After ultracentrifugation, the supernatants constituting the nuclear protein extracts were used for western blots.

Western blot

10 μ g (total extracts) and 20 μ g (nuclear extracts) of lysates were loaded onto a 4%–12% Bis-Tris SDS-PAGE gel (Life Technologies) and transferred to a PVDF membrane (Bio-Rad). Western blots were performed according to standard procedure. We used the following antibodies: α -AKT (CST, 4685), α -AKT (pS473) (Santa Cruz, sc-7985), α -GR (Santa Cruz, sc-393232), α -CRY1 (Abcam, ab104736), and α -CRY2 (kindly supplied by Katja Lamia). Secondary antibodies were: α -rabbit IgG (Santa Cruz, sc-2317), α -mouse IgG (BioRad, 170-6516) and α -guinea pig IgG (Santa Cruz, sc2438).

ChIP-MS

For ChIP experiments followed by mass spectrometry (ChIP-MS), ChIP was performed as described above with minor modifications. For each biological condition, liver samples from 3 mice were pooled. Chromatin was sonicated to an average size of 200bp. Antibody-bait complexes were bound by protein G-coupled Dynabeads (Life Technologies) and washed three times with wash buffer A (50mM HEPES pH 7.5, 140mM NaCl, 1% Triton), once with wash buffer B (50mM HEPES pH 7.5, 500mM NaCl, 1% Triton) and twice with TBS. Precipitated proteins were eluted with an on-bead digest as described before (Hein et al., 2015). Beads were incubated for 30min with elution buffer 1 (2M Urea, 50mM Tris-HCl (pH 7.5), 2mM DTT, 20 μ g/ml Trypsin) followed by a second elution with elution buffer 2 (2M Urea, 50mM Tris-HCl (pH 7.5), 10mM Chloroacetamide) for 5min. Both eluates were combined and incubated overnight at room temperature. Tryptic peptide mixtures were acidified with 1% TFA and desalted with Stage Tips containing 3 layers of C18 reverse phase material and analyzed by mass spectrometry.

Peptides were separated on 50-cm columns packed in-house with ReproSil-Pur C18-AQ 1.9 μm resin (Dr. Maisch GmbH). Liquid chromatography was performed on an EASY-nLC 1000 ultra-high-pressure system coupled through a nanoelectrospray source to a Q-Exactive HF mass spectrometer (Thermo Fisher Scientific). Peptides were loaded in buffer A (0.1% formic acid) and separated applying a non-linear gradient of 5%–60% buffer B (0.1% formic acid, 80% acetonitrile) at a flow rate of 250nl/min over 105min. Data acquisition switched between a full scan and 15 data-dependent MS/MS scans. Multiple sequencing of peptides was minimized by excluding the selected peptide candidates for 25 s. All other settings were set as previously described (Scheltema et al., 2014).

Missing values were imputed from a normal distribution applying a width of 0.2 and a downshift of 1.8 standard deviations. Significant outliers were defined by permutation-controlled Student's t test (FDR < 0.02, $s_0 = 1$) comparing triplicate ChIP-MS samples for each antibody and biological condition.

QUANTIFICATION AND STATISTICAL ANALYSIS

Animal experiments were randomized in control and HFD treated groups, individual data point are represented in the plots. In all cases, two tailed tests with P values less than 0.05 were significant. For ChIP-qPCR, multiple t test was performed with $p < 0.05$ ($n = 2$ –6 per group). For differences between groups in Rlog counts, multiple t test was run, with $p < 0.05$ ($n = 3$ per group).

BIOINFORMATICS (SEE FIGURE S1G)

ChIP-Seq

Pre-processing

ChIP-Seq FASTQ files were mapped against the mouse mm9 genome with BWA version 7.12 using the MEM algorithm (Li and Durbin, 2010). Duplicate reads were removed using samtools version 0.1.19. Multi mapping reads were removed with bamtools version 2.4.0 using a read threshold of MAPQ > = 24 (Barnett et al., 2011).

Adjusting sequencing depth

Sequencing read depth was adjusted for by down sampling each replicate BAM file to the replicate with the lowest read count (Table S3).

Peak calling

Macs2 version 2.1.1 was used for peak calling on the replicates using liver genomic DNA as input control (Feng et al., 2011). The peak calling cutoff was set to FDR = 0.05. Apart from generating narrow peak files, input normalized read density distributions (Bedgraph) were used for further analysis. Peak boundaries were set by extending the peak summit in either direction by its corresponding library size (calculated from the Bioanalyzer) for each replicate.

Signal artifacts

Peaks falling within pathological repeat elements like satellites, centromeres and telomeric repeats including the ENCODE published black listed regions (<https://sites.google.com/site/anshulkundaje/projects/blacklists>) were removed from the peak list using Bedtools version v2.25.0 (Quinlan, 2014).

Replicate reproducibility

A customized version of the ENCODE IDR pipeline was used to account for paired-end reads. Pseudo replicates and pairwise correlation analyses were performed among replicate pairs. Peaks within a 200bp summit to summit neighboring distance and $\geq 50\%$ boundary overlap were merged and marked as confident peaks. Read density plots and Pearson correlation were also calculated for each replicate to ensure reproducibility. Bedtools version v2.25.0 (Quinlan, 2014) was used to perform the overlap analysis. R version 3.2.3 and Bioconductor were used to create Pearson correlation plots.

Peak Unions

Peak union tables with unique genomic locations from both control and HFD groups were created for GR, STAT5, PPAR α , GR-Dex, and H3K27ac datasets. These tables were then combined into a unified peak union with unique ranges across the genome and containing overlapping HFD and control peak information, including the tag count. This table was then used to calculate the peak distribution across the genome and identify peaks of interest, calculating IP efficiency normalization factors.

IP efficiency normalization

ChIP peaks near the promoters of non-changing genes were selected as 'static peaks' (based on RNA-Seq non-differential expression across all HFD and control samples; and based on performance in the different ChIP experiments) (Table S4). Normalization factors for each replicate were calculated as follows: first, the mean of the non-changing static peaks was calculated for a given region of overlap between peaks (h). Then for a given region (n), the mean of each sample was normalized to a particular signal (h_n). Then the normalization factor for each sample would be: $F_n = \text{summation of } (h_n) / \text{total number of control peaks}$. The count estimate for sample (i) would be: $n_i = F_n * x_i$. The normalization factors for each replicate were then used to account for differences in IP efficiency (Table S3). This method is based on the THOR package (Allhoff et al., 2016).

Normalized peak union

Bedgraphs were normalized with the scaling factors obtained from the IP efficiency calculation. Peak calling was then performed on the normalized Bedgraphs with macs2 version 2.1.1 using the bdgpeakcall module with a threshold of p value $1e-5$. To account for

false positives, we selected the peaks based on their overlap with the original union. The normalized peak union was then created with normalized tag counts. UCSC tracks were also created using the normalized Bedgraphs.

Normalized read density heatmaps

Normalized bedgraphs were used to plot the read density map near the union peak centers using deepTools version 2.2.4. Replicate groups per time point were first merged using UCSC tools bedGraphToBigWig and bigWigMerge (http://hgdownload.cse.ucsc.edu/admin/exe/macOSX.x86_64/). Then the deepToolscomputeMatrix tool was used, followed by the plotHeatmap tool.

Peak annotation

Peak annotation was performed with HOMER version v4.8 (Heinz et al., 2010). The GENCODE database for mm9 (Release M1) was used as a reference for assigning feature level annotation. Annotated peaks for GR, STAT5, PPAR α , and H3K27ac are listed in Table S5.

Motif discovery

Two different methods were used for motif discovery: HOMER version v4.8 and a motif analysis based on position site specific matrix models to quantify the utilization of specific hormone response elements (Wilson et al., 2017; Wilson et al., 2016). The ChIP-Seq data was aligned using the ucsc_mm9 reference frame. For individual motif occurrences, a position specific matrix served to compute a log-likelihood ratio score, p values and q values.

Pathway and GO annotation

Pathway enrichment and gene ontology annotation were performed by using the Enrichr and GREAT websites, respectively (Kuleshov et al., 2016; McLean et al., 2010 #323).

RNA-Seq

Pre-processing

RNA-Seq FASTQ files were mapped against the mouse mm9 genome with the STAR v2.4.2a aligner (Dobin et al., 2013). The GENCODE mm9 genome annotation was used. Format conversions were performed using samtools v1.3.1 (Li et al., 2009). The featureCounts program (Liao et al., 2014) was used to count reads located within an exon, do not overlap multiple features, with a threshold of MAPQ ≥ 4 and are not chimeric.

Normalization and differential expression analysis

The read count matrix was fed into the DESeq2 v1.23.10 program (Love et al., 2014), and variance stabilization was performed to obtain a normalized data matrix. Differential gene expression analysis was performed using a model that quantifies the effect of diet, genotype, time, and their interactions, comparing the different diet-genotype-time groups with each other. The Dex treatment experiment was performed at a single time point. In this case our design formula was: design = \sim diet + treatment + diet:treatment. The number of biological replicates is stated for each comparison (Table S6).

Oscillating transcript analysis

After normalization, transcript rhythmicity was determined by JTK cycle (Hughes et al., 2010) through the MetaCycle R package (Wu et al., 2016). Circadian cycling was determined over a period of 24h and significant transcripts were selected by using an adjusted p value < 0.05 . The groups used for the analysis were hepatocyte-specific *Alb-Cre* \times *GR^{fl/fl}* and littermate *GR^{fl/fl}* controls, placed on HFD feeding for 12 weeks or control diet (Table S6).

ChIP-MS

Raw mass spectrometry data were analyzed with MaxQuant (version 1.5.3.29) and Perseus (version 1.5.3.0) software packages. Peak lists were searched against the mouse UniprotFASTA database (2015_08 release) combined with 262 common contaminants by the integrated Andromeda search engine. False discovery rate was set to 1% for both peptides (minimum length of 7 amino acids) and proteins. 'Match between runs' with a maximum time difference of 0.7min was enabled. Relative proteins amounts were determined by the MaxLFQ algorithm, with a minimum ratio count of two (Table S7) (Cox et al., 2014).

DATA AND CODE AVAILABILITY

The ChIP-Seq and RNA-Seq datasets generated during this study are available at the GEO (NCBI) database under the SuperSeries accession number GEO: GSE108690. Proteomics data have been deposited in the PRIDE archive (EBI): accession PRIDE: PXD014030. All other NGS and mass spec data in the paper are available in supplemental tables.

Supplemental Information

Cistronic Reprogramming of the Diurnal

Glucocorticoid Hormone Response by High-Fat Diet

Fabiana Quagliarini, Ashfaq Ali Mir, Kinga Balazs, Michael Wierer, Kenneth Allen Dyar, Celine Jouffe, Konstantinos Makris, Johann Hawe, Matthias Heinig, Fabian Volker Filipp, Grant Daniel Barish, and Nina Henriette Uhlenhaut

Supplemental Information

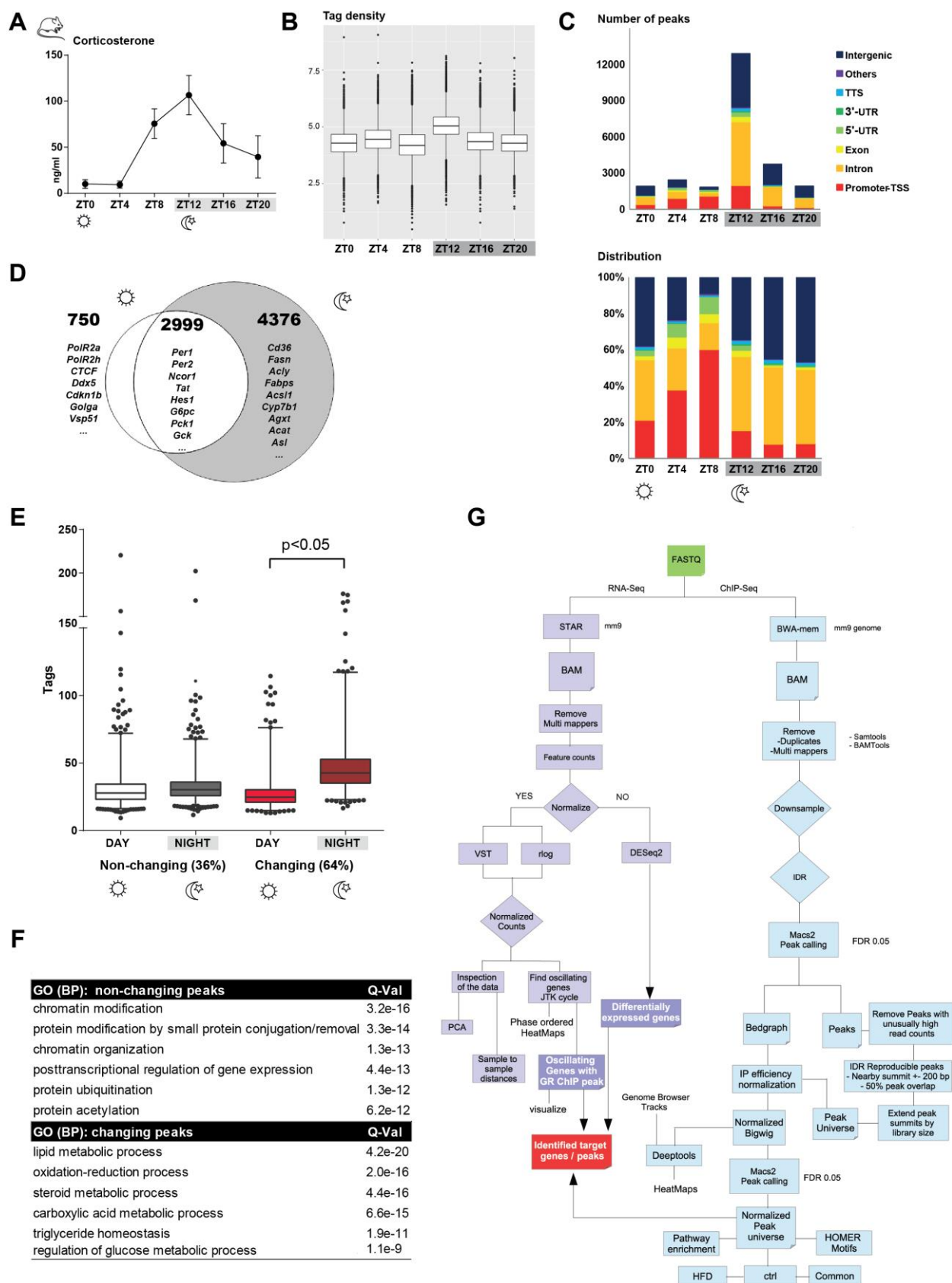
Cistronic reprogramming of the diurnal glucocorticoid hormone response by high fat diet

Fabiana Quagliarini et al.

corresponding author / lead contact:

N. Henriette Uhlénhaut, henriette.uhlenhaut@helmholtz-muenchen.de

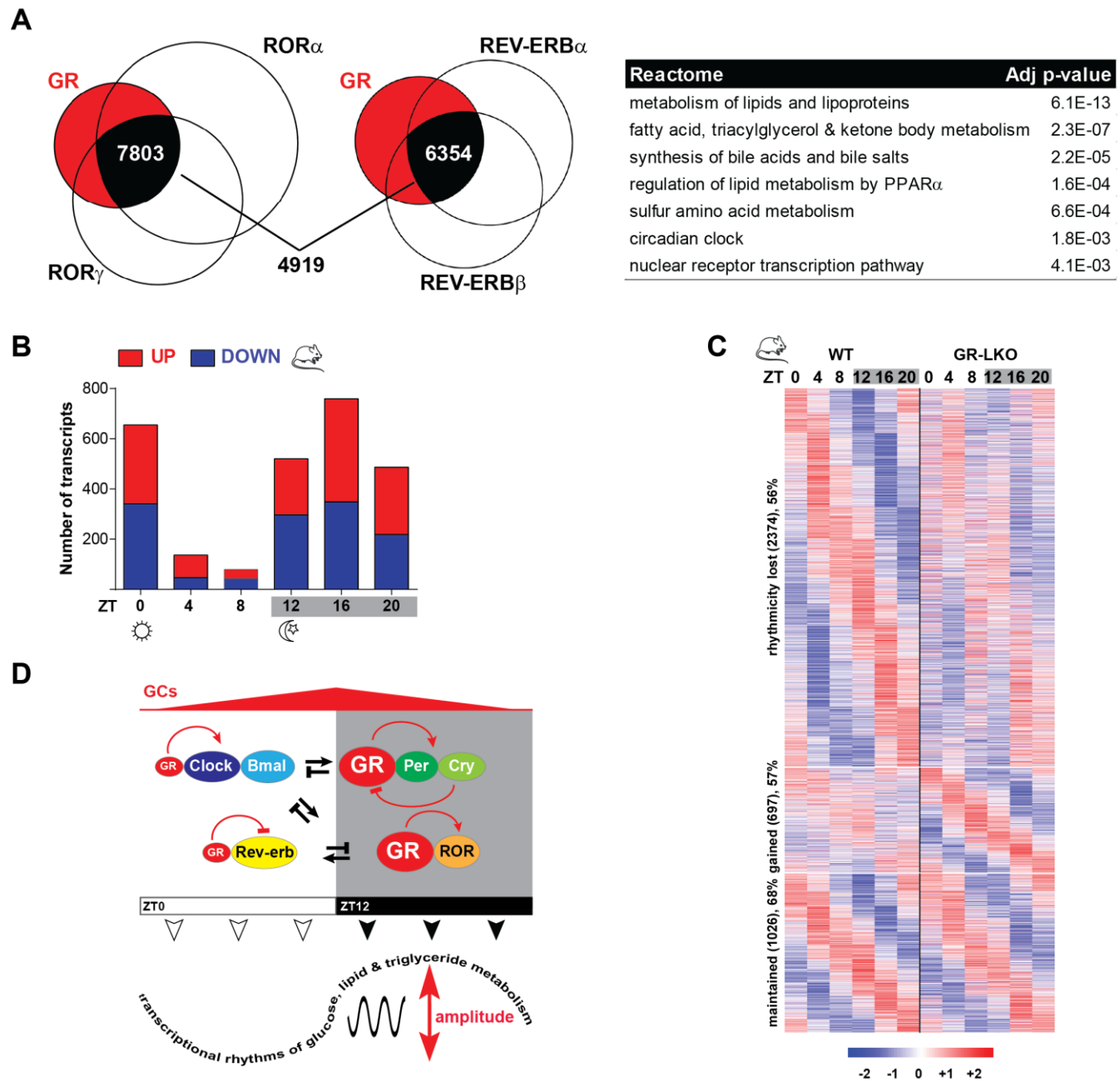
Figure S1, related to Figure 1.



Supplementary Figure 1, related to Figure 1. Differential genomic binding of GR during the day and night cycle in mouse livers

(A) Serum corticosterone levels, measured from euthanized mice every 4h (ZT0-20) by ELISA. Values are represented as mean \pm SD; n=3. (B) Box plot of log2-transformed read densities of GR ChIP-Seq in mouse livers from ZT0-20. (C) The total number of reproducible peaks and the genomic peak distribution for ZT0-20. (D) Venn diagram showing the number and examples of genes associated with GR binding during the Day (ZT0,4,8) and the Night (ZT12,16,20). (E) The tag density of the 2,999 'common' peaks in panel S1D was averaged separately for the Day (ZT0,4,8, n=6), and for the Night (ZT12,16,20, n=6), and statistically sub-grouped into non-changing ($p>0,05$; 36%) and changing ($p<0,05$; 64%) (significance by multiple t-test). (F) Enriched GO terms for peaks near genes with either constant or differential binding, see S1E. (G) Overview of the bioinformatic analysis pipelines used for ChIP- and RNA-Seq data.

Figure S2, related to Figure 2.



Supplementary Figure 2, related to Figure 2. GR binding overlaps with core clock factors to generate transcriptional rhythms

(A) Overlap of GR with ROR α / γ and REV-ERB α / β cistromes. GR universe (sum of all GR ChIP-Seq peaks from all time points) intersection with ROR α / γ universes (ZT10 and ZT22; Zhang Y et al., Fang B et al.) and REV-ERB α / β universes (ZT8; Cho H et al). 4,919 sites are bound altogether by GR-RORs-REV-ERBs. Functional annotation (Enrichr) of genes near overlapping sites. (B) Number of deregulated transcripts in GR-LKO (*Alb-Cre* x *GR^{fl/fl}*) livers at ZT0, 4, 8, 12, 16 and 20. Differential gene expression between GR-LKO and floxed littermates was calculated per time point using DESeq2 (n=3, adj p<0.05). (C) Phase sorted heatmap of all oscillating transcripts in livers from control and GR-LKO mice, for ZT0-20. Rhythmicity was determined using JTK Cycle (period 24, adj p<0.05), n=3. (D) Schematic depicting the interactions of GR with both the core and the ancillary clock machinery to generate rhythmic output.

A

B

C

D

E

F

G

H

RNA

I

J

K

L

M

N

O

P

Q

R

S

T

U

V

W

X

Y

Z

AA

AB

AC

AD

AE

AF

AG

AH

AI

AJ

AK

AL

AM

AN

AO

AP

AQ

AR

AS

AT

AU

AV

AW

AX

AY

AZ

BA

BB

BC

BD

BE

BF

BG

BH

BI

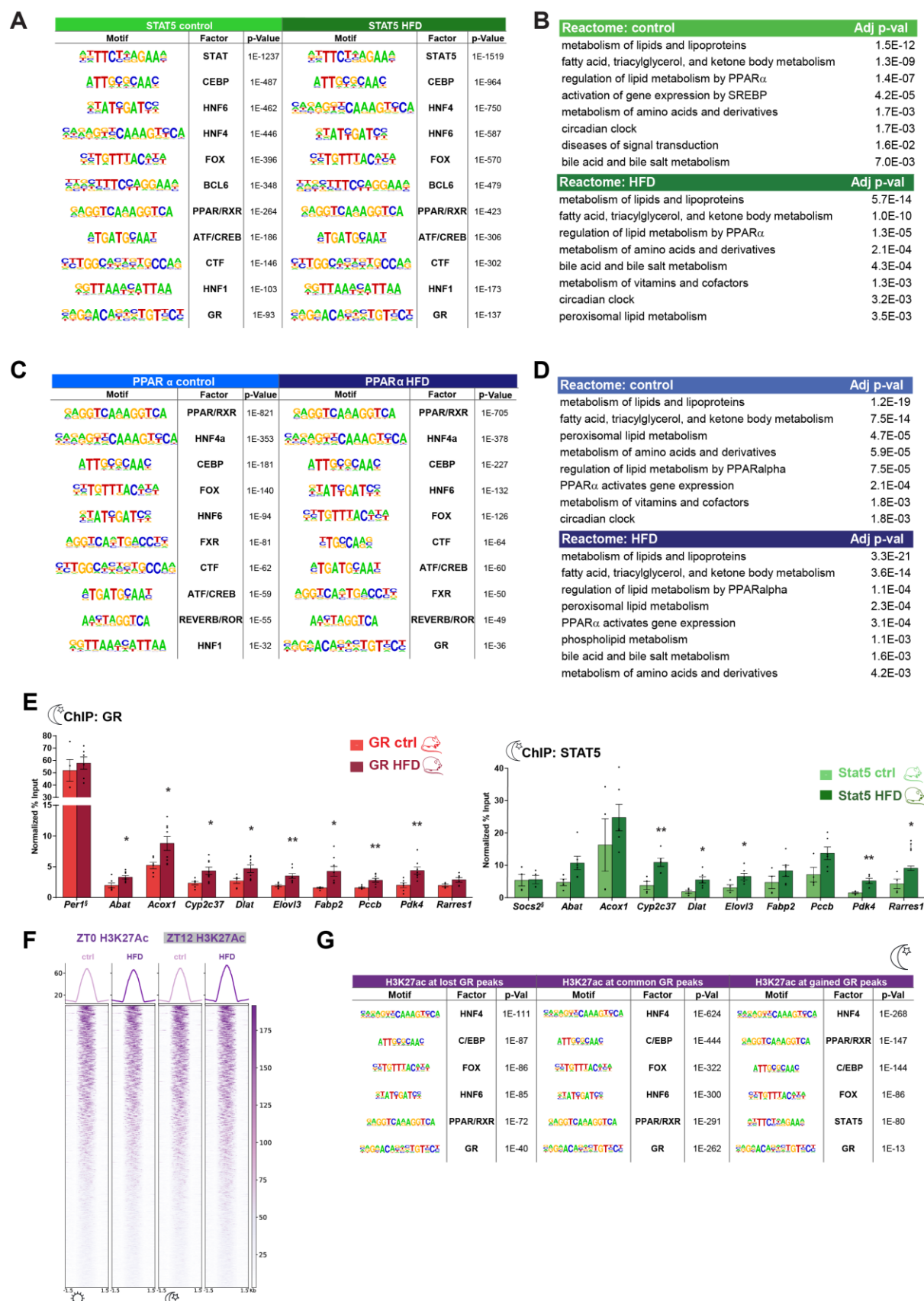
BJ

Supplementary Figure 3, related to Figure 3. GR cistromes are reprogrammed by HFD

(A) Heatmap of GR genome-wide binding in control and HFD livers for ZT0-20, analogous to Figures 1B and 3A. (B) The total number of reproducible GR peaks and their genomic distribution for ZT0-20 on HFD. (C) Venn diagram showing called GR peaks during the Day (ZT0,4,8) and Night (ZT12,16,20). GO annotation (GREAT) of the genes nearest to the 3,258 'Day' binding sites and the 16,954 'Night-only' binding sites. (D) Weight gain from C57BL/J mice after 12 weeks of HFD feeding (58% fat) compared to controls fed LFD (11% fat). Values are represented as mean \pm SD. (E) Western Blots of AKT in total liver extracts from control and HFD mice at ZT12. (F) Serum corticosterone levels of control and HFD mice measured by ELISA. Blood was taken every 4h. Values are mean \pm SD, n=3. (G) Serum corticosterone levels from HFD and control mice either at ZT0 (GC trough) or at ZT12 (GC peak). Values are mean \pm SD, n=10-15. (H) Heatmap of transcripts deregulated by HFD during the day (ZT0,4,8) and associated with 'gained' GR binding from Figure 3E (9,354 peaks). Differential gene expression in livers from HFD fed and control wildtype mice was calculated by using DESeq2 (n=3, adj p<0.05) as described. Pathway annotation was performed for transcripts either up- or down-regulated in HFD livers. (I) Temporal protein accumulation of GR, CRY1, and CRY2 in HFD and control livers. Western blots on nuclear extracts; naphtol blue black staining was used as loading control. Corresponding mean densitometry values, normalized to the loading control. Data for each time point are mean \pm SD, n=2.

****** P <0.01 (two tailed t test).

Figure S4, related to Figure 4.



Supplementary Figure 4, related to Figure 4. GR, PPAR α and STAT5 signaling pathways intersect at functional enhancers

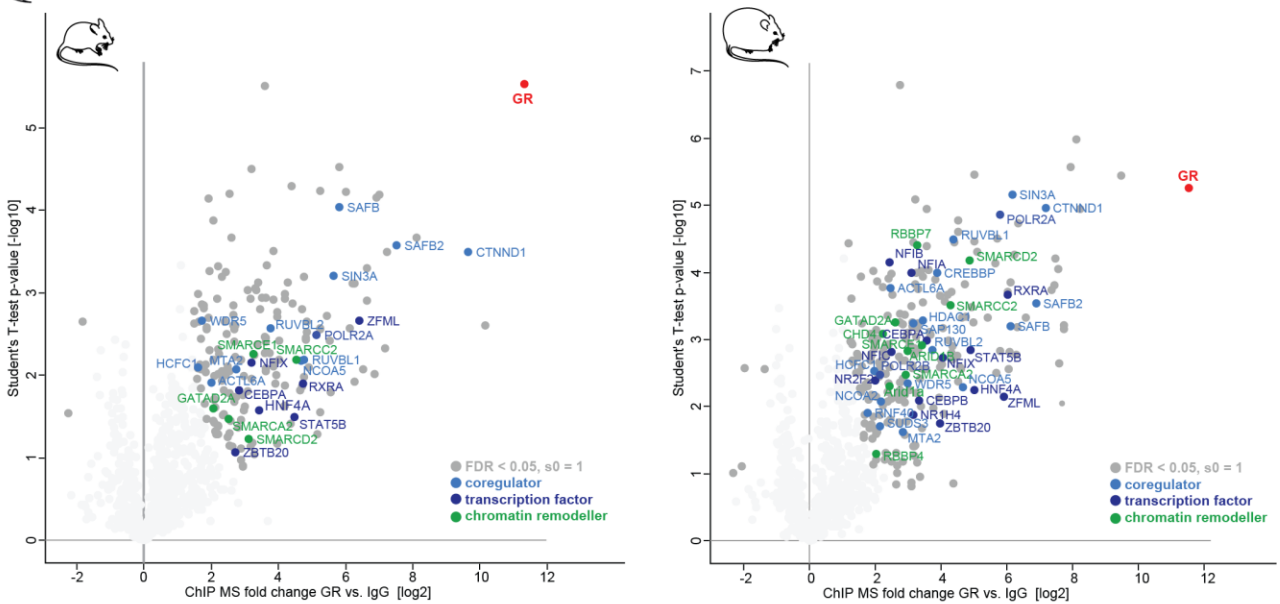
(A) Motif analyses of the control and HFD liver cistromes for STAT5 (A) and PPAR α (C) at ZT12. Functional annotation of the genes near STAT5 (B) and PPAR α (D) binding sites in HFD and control livers. (E) GR and STAT5 ChIP-qPCR data from control and HFD livers. § The *Per1* and *Socs2* loci are non-changing sites, the other loci showed increased occupancy for both factors with ChIP-seq. Enrichment was calculated over a negative locus. Values are mean \pm SEM (n=4-8). (F) Total H3K27ac profiles from control and HFD livers at ZT0 and ZT12. Each row shows the normalized unique ChIP-Seq tag counts for H3K27ac ordered by signal strength (n=2 mice per group). (G) Motif analysis for H3K27ac peaks overlapping with 'lost' (3,031 out of 3,076), 'common' (10,520 out of 10,616), or 'gained' (9,291 out of 9,354) GR peaks as described in Figure 3E.

* $P < 0.05$, ** $P < 0.01$ (two tailed t test).

Figure S5, related to Figure 5.

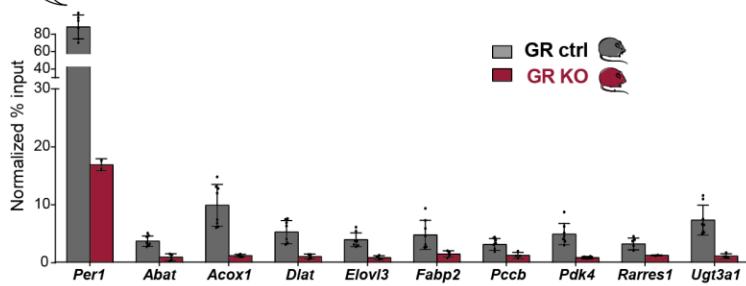
A

ChIP: GR



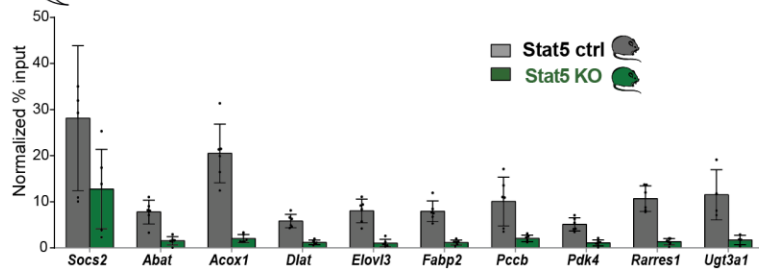
B

ChIP: GR in GR-LKO



C

ChIP: STAT5 in Stat5-LKO



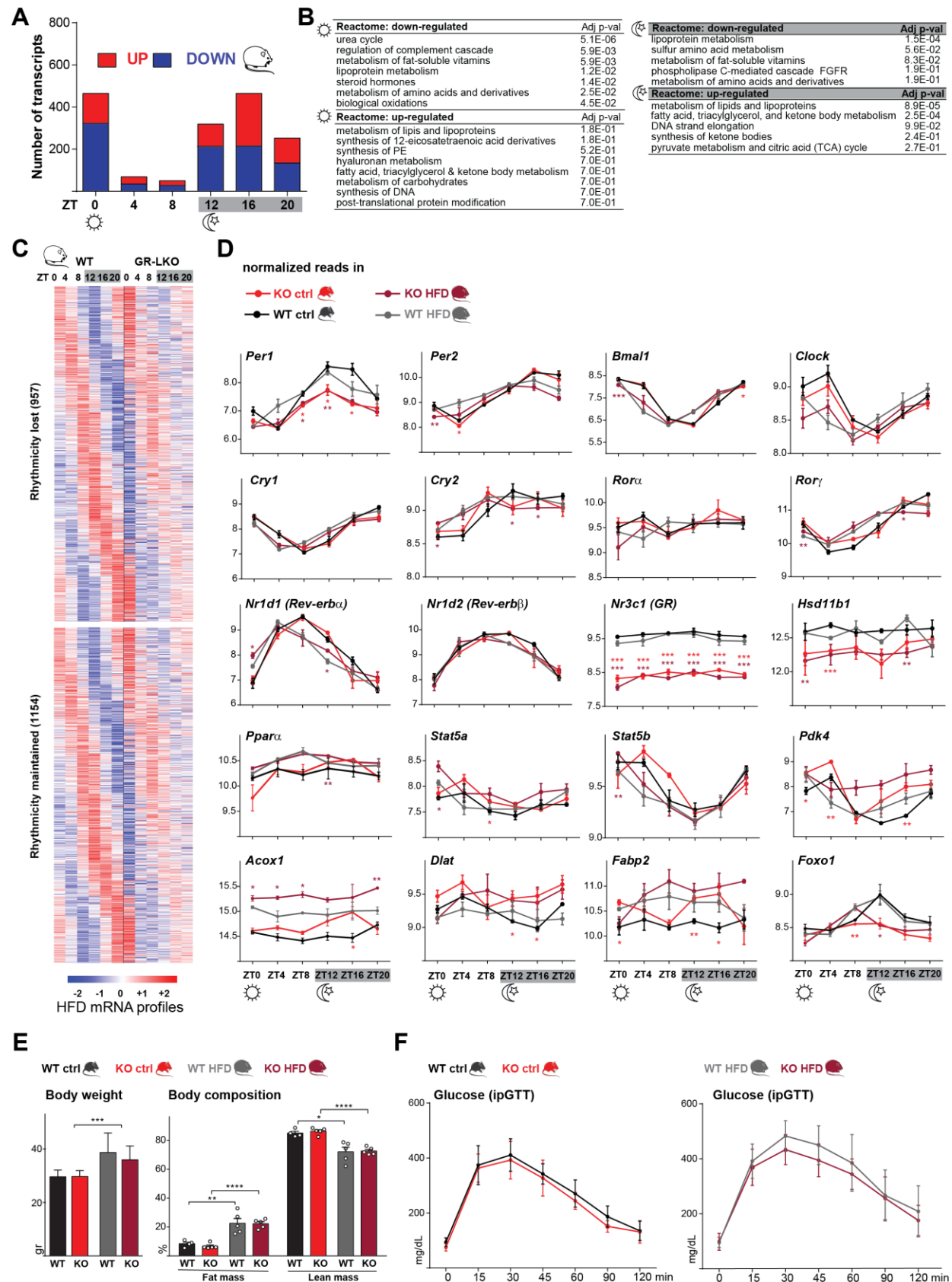
Supplementary Figure 5, related to Figure 5. Cistronic reprogramming by HFD depends on STAT5 occupancy

(A) Volcano plot of significantly enriched proteins in GR IP samples versus IgG, in control and HFD livers. Proteins of special interest are colored, dark grey: Fisher's exact test (FDR<0.05, s0=1); n=3.

(B) GR ChIP-qPCR analysis in GR mutant (*Alb-Cre x GR^{fl/fl}*) and control livers (*GR^{fl/fl}*) after 12 weeks of HFD. Enrichment was calculated over a negative locus. Values are mean±SEM (n=2-8 per group; all loci are significantly different between the two groups, multiple t-test).

(C) STAT5(a/b) ChIP-qPCR analysis in Stat5 knockout (*Alb-Cre x Stat5^{fl/fl}*) and control (*Stat5^{fl/fl}*) livers after 12 weeks of HFD. Enrichment was calculated over a negative locus. Values are mean± SEM (n=6 per group; all loci are significantly different between the two groups).

Figure S6, related to Figure 6.



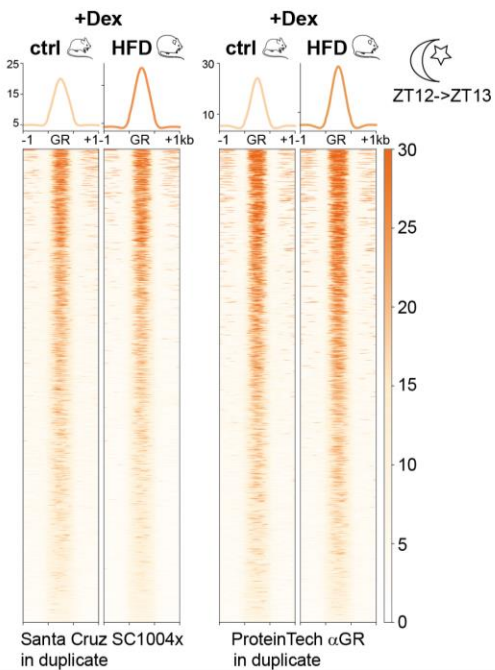
Supplementary Figure 6, related to Figure 6. GR liver specific deletion leads to deregulation of glucose and triglyceride metabolism

(A) Number of deregulated transcripts in GR-LKO (*Alb-Cre* x *GR^{fl/fl}*) livers at ZT0, 4, 8, 12, 16 and 20 after 12 weeks of HFD. Differential gene expression between GR-LKO and floxed littermates was calculated per time point using DESeq2 (n=3, adj p<0.05). (B) Pathway annotation for transcripts either up- or down-regulated in GR-LKO during the 'Day' (ZT0, 4, 8) and during the 'Night' (ZT12, 16, 20) as defined in Figure 6A. (C) Phase sorted heatmap of all oscillating transcripts around the clock in livers from control and GR-LKO mice on HFD. Rhythmicity was determined using JTK Cycle (period 24, adj p<0.05), n=3. (D) Rlog transformed counts from normalized RNA-Seq data of selected transcripts in livers from GR-LKO and floxed littermates, fed either high fat or control diet. Values are mean±SEM (n=3). (E) Body weight (n=20 per group) and body composition analysis of 20-22 week old GR-LKO male mice and littermate controls (*GR^{fl/fl}*), values are mean ± SD (n=20). (F) i.p. glucose tolerance tests (GTT) in 18-20 week old male mice, after 10 weeks of HFD or control diet. Values are mean±SD (n=4-15).

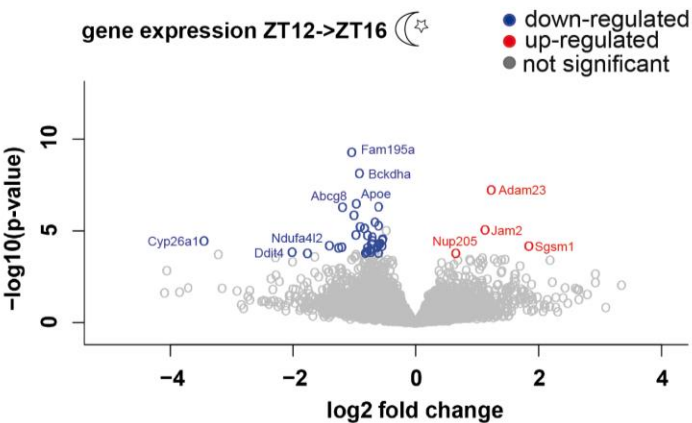
P*<0.05, *P*<0.01, *** *P*<0.001, **** *P*<0.0001 (two tailed *t* test).

Figure S7, related to Figure 7.

A



B



Supplementary Figure 7, related to Figure 7. Ligand independent genomic responses on HFD

(A) Heatmaps showing GR genomic binding in Dex treated livers on control and HFD. Dex was injected at ZT12 and mice sacrificed at ZT13. Two different GR antibodies (Santa Cruz, SC-1004x and Protein Tech, 24050-1-AP) were used. (B) Volcano plot showing transcripts differentially responding to Dex treatment in HFD versus control diet (n=2-3, adj p<0.05). Mice were injected with Dex at ZT12 and livers were processed at ZT16. Genes significantly associated with diet-dependent differential responses are shown in blue (down-regulated) and red (up-regulated).

Table S1, related to Figure 2.

Gene Name	Peak			Time Point	Position	+DEX (Log2FC)
<i>Clock</i>	chr5	76732589	76734428	ZT0;4;8;12	Promoter	0,78
	chr5	76734709	76735615	ZT12	Intergenic	
<i>Arntl</i>	chr7	120350700	120351665	ZT0;4;8;12;16	Intron 1	nc
	chr7	120403794	120404700	ZT12;16	Intron 2	
<i>Cry1</i>	chr10	84647390	84648345	ZT4	Promoter	nc
	chr10	84652487	84653585	ZT0;12	Intergenic	
<i>Cry2</i>	chr2	92261760	92262673	ZT12	Intron 2	1,2
	chr2	92272274	92273180	ZT12	TTS	
<i>Per1</i>	chr11	68910121	68911027	ZT12	Promoter	1,97
	chr11	68912491	68913397	ZT0;4;8;12;16;20	Intergenic	
<i>Per2</i>	chr1	93332654	93333565	ZT12	Intron 1	-1,58
	chr1	93336185	93337113	ZT0;12	Intron 4	
	chr1	93342379	93343285	ZT12	Intron 7	
	chr1	93352188	93353154	ZT0;4;12;16;20	intron 9	
	chr1	93359681	93360587	ZT12	Intergenic	
<i>Rora</i>	chr9	68957620	68958540	ZT8;12	Promoter	1,41
	chr9	69031405	69032335	ZT12;16	Intron 1	
	chr9	69132473	69133470	ZT0;12;16	Intron 1	
	chr9	69135683	69136589	ZT12;16	Intron 1	
	chr9	69137114	69138020	ZT12	Intron 1	
	chr9	69154162	69155177	ZT12	Intron 1	
	chr9	69181649	69182582	ZT12;20	Intron 1	
	chr9	69186770	69187676	ZT12	Intron 1	
	chr9	69160803	69161831	ZT12	Intron 1	
	chr9	69179267	69180274	ZT12	Intron 2	
	chr9	69180284	69181190	ZT12	Intron 2	
<i>Rorc</i>	chr3	94171203	94172228	ZT12;16	Intron 1	nc
	chr3	94177426	94178332	ZT12	Intergenic	
<i>Nr1d1</i>	chr11	98644175	98645081	ZT12	Intergenic	-1,97
<i>Nr1d2</i>	chr14	19071427	19072196	ZT8	Promoter	nc

Table S2, related to STAR Methods. Primer list for ChIP-qPCR.

Name	Strand	Sequence
<i>Per1</i>	Forward Reverse	GTAGGTCCCGCAAAGAGAACC GACAGCGGTCCTGTACAAAAG
<i>Negative ctrl</i>	Forward Reverse	GCTGGCAGAATAGCATCCG TGATGAAGCACTCGTTGAGGC
<i>Socs2</i>	Forward Reverse	CTCGGGAACAAGGAGAAGTC GAGAAGAGGGGCTGCTATTC
<i>Rarres1</i>	Forward Reverse	GTGGGTTCTAAGACCTGAGGG CACACTTTCCCTGTTTCCAGC
<i>Abat</i>	Forward Reverse	TGGCACACAACCAATCCCAG TGACACACTACCCATTCCAGC
<i>Dlat</i>	Forward Reverse	AACTATGGAGTAACAATGTGGG TAGGCAGCAGTAGTGAGAAAC
<i>Elovl3</i>	Forward Reverse	CCAAACTCAGAGAGAAAGCAG CAGCCAGTGTCTAGAAATCC
<i>Pdk4</i>	Forward Reverse	CATCAGGTCAAGGTTTGTACTC ATGTGTGTGGACTCTAGTTTCC
<i>Acox1</i>	Forward Reverse	CTGTTGATTTTACTGGAACCC TAGCCAACGACAATGAACC
<i>Cyp2c37</i>	Forward Reverse	GGGCAATGTGCATCACAACA TGTTGAACTTTGTGATACGGGC
<i>Fabp2</i>	Forward Reverse	ATGTGAGGCGGTTAGGTTATC TCCAGTCCTGTCCACTAGAGAG
<i>Pccb</i>	Forward Reverse	AAGCTGGTAGCAGTCACAGG AAGTCCTTGTTCTGTGTGGC
<i>Ugt3a1</i>	Forward Reverse	TCTCTACTCTGAGTTTCCTGGTC CCTGGACTCCTCCTTTCAGAG

Table S3, related to STAR Methods. Summary of the results from our ChIP-Seq bioinformatics pipeline.

Type	Code	Diet	Sample	Type of sequence	# of mapped reads	% of mapped reads	# of mapped reads w/out duplicates	% of duplicates	# of uniquely mapped reads (>24)	% of reads used	# macs2peaks (FDR-0.05)	Scaling factor
GR	ZT0	CTRL	Rep1	pair-end	49821035	96.77	36882891	25.97	33071118	66.38	5890	0.1856
GR	ZT0	CTRL	Rep2	pair-end	23545907	98.11	20088577	14.68	18008935	76.48	4971	0.1739
GR	ZT4	CTRL	Rep1	pair-end	27970302	97.91	23730832	15.16	21247124	75.96	3619	0.1681
GR	ZT4	CTRL	Rep2	pair-end	47762630	93.18	26104183	45.35	22607447	47.33	18101	0.1261
GR	ZT8	CTRL	Rep1	single-end	29989335	94.24	21327340	28.88	18261739	60.89	8360	0.1289
GR	ZT8	CTRL	Rep2	pair-end	29090717	98.23	22264367	23.47	19774145	67.97	2752	0.2454
GR	ZT12	CTRL	Rep1	single-end	29182848	95.68	20801305	28.72	17938845	61.47	23534	0.1464
GR	ZT12	CTRL	Rep2	pair-end	39561957	97.19	25370018	35.87	22355227	56.51	24403	0.1872
GR	ZT16	CTRL	Rep1	pair-end	28002841	97.36	22791872	18.61	20501937	73.21	9567	0.1815
GR	ZT16	CTRL	Rep2	pair-end	45136520	99.22	38494278	14.72	34886926	77.29	6512	0.1588
GR	ZT20	CTRL	Rep1	pair-end	38074861	98.74	32039673	15.85	29057486	76.32	7484	0.1328
GR	ZT20	CTRL	Rep2	pair-end	17373101	98.22	15423999	11.22	13896001	79.99	3133	0.1618
GR	ZT0	HFD	Rep1	pair-end	19392586	98.47	16113698	16.91	14503304	74.79	5862	0.1845
GR	ZT0	HFD	Rep2	pair-end	68835259	97.43	54958388	20.16	50463935	73.31	23878	0.0874
GR	ZT4	HFD	Rep1	pair-end	28712926	95.21	22306944	22.31	19946682	69.47	1998	0.1788
GR	ZT4	HFD	Rep2	pair-end	25059275	97.53	21487565	14.25	19355293	77.24	12197	0.1173
GR	ZT8	HFD	Rep1	pair-end	39387334	98.68	31754704	19.38	28638566	72.71	2556	0.2454
GR	ZT8	HFD	Rep2	pair-end	35021832	97.99	28614984	18.29	26078073	74.46	25666	0.0827
GR	ZT12	HFD	Rep1	pair-end	41336379	98.6	30518017	26.17	23356466	56.5	29045	0.1549
GR	ZT12	HFD	Rep2	pair-end	76748986	96.67	54282974	29.27	49718202	64.78	40934	0.1067
GR	ZT16	HFD	Rep1	pair-end	38262648	98.45	28189873	26.33	21704393	56.72	38972	0.1002
GR	ZT16	HFD	Rep2	pair-end	56862314	98.66	34383965	39.53	30136554	53	12811	0.1610
GR	ZT20	HFD	Rep1	pair-end	61272128	99.07	46963210	23.35	42225476	68.91	8956	0.1407
GR	ZT20	HFD	Rep2	pair-end	69727647	98.59	49583131	28.89	45489201	65.24	10140	0.1392
GR	.	mixed	input	pair-end	192581321	99.35	124787275	35.2	111042277	n/a	.	.
STAT5	ZT12	HFD	Rep1	pair-end	25110524	94.47	15219321	39.4	13349164	53.16	30559	0.0834
STAT5	ZT12	HFD	Rep2	pair-end	64374196	97.81	44882152	30.2	40388712	62.74	33465	0.0787
STAT5	ZT12	CTRL	Rep1	pair-end	32526033	96.27	20636095	36.5	18002967	55.35	11396	0.1452

STAT5	ZT12	CTRL	Rep2	pair-end	42774150	98.30	25855654	39.5	22747958	53.18	19765	0.1188
PPARA	ZT12	CTRL	Rep1	pair-end	48125505	98.67	28087183	41.6	11724029	24.36	12701	0.1030
PPARA	ZT12	CTRL	Rep2	single-end	.	.	16352720	.	13539989	.	6093	0.1030
PPARA	ZT12	HFD	Rep1	pair-end	43035390	98.49	25248145	41.3	11005152	25.57	17079	0.1036
PPARA	ZT12	HFD	Rep2	single-end	.	.	12388782	.	10192046	.	6545	0.0915
DEX	ZT0	CTRL	Rep1	pair-end	.	98.72	35021253	.	31254219	.	1605	0.2530
DEX	ZT0	CTRL	Rep2	pair-end	.	97.41	33974624	.	30296455	.	12568	0.1271
DEX	ZT0	HFD	Rep1	pair-end	.	98.35	34834975	.	31120695	.	7485	0.1721
DEX	ZT0	HFD	Rep2	pair-end	.	97.89	35232304	.	31235195	.	2031	0.1570
DEX (PT)	ZT12	CTRL	Rep1	pair-end	31535073	99.33	24005225	23.9	21327120	67.6	15954	0.2933
DEX (PT)	ZT12	CTRL	Rep2	pair-end	44756966	99.41	33313453	25.6	30076082	67.2	37083	0.1293
DEX (PT)	ZT12	HFD	Rep1	pair-end	31491633	99.35	25802125	18.1	23126212	73.4	21829	0.1718
DEX (PT)	ZT12	HFD	Rep2	pair-end	32608848	99.42	24545669	24.7	22269509	68.3	28192	0.1421
DEX	ZT12	CTRL	Rep1	pair-end	37362882	97.86	27401154	26.7	24273134	65	14404	0.1393
DEX	ZT12	CTRL	Rep2	pair-end	29785772	98.33	24066597	19.2	21682700	72.8	34023	0.0675
DEX	ZT12	HFD	Rep1	pair-end	31928484	94.16	25681532	19.6	22524924	70.5	21246	0.1176
DEX	ZT12	HFD	Rep2	pair-end	28495535	98.77	22581987	20.8	20291786	71.2	32357	0.1288
H3K27ac	ZT0	CTRL	Rep1	pair-end	86001548	99.09	41521207	51.7	38241993	44.5	46594	0.1738
H3K27ac	ZT0	CTRL	Rep2	pair-end	81914623	99.40	49961499	39	46244532	56.5	41501	0.1640
H3K27ac	ZT0	HFD	Rep1	pair-end	73353936	99.22	41732804	43.1	38653402	52.7	47273	0.1485
H3K27ac	ZT0	HFD	Rep2	pair-end	91379344	99.31	58779485	35.7	54636101	59.8	45622	0.1602
H3K27ac	ZT12	CTRL	Rep1	pair-end	83933293	99.25	56562839	32.6	52843661	63	43439	0.1682
H3K27ac	ZT12	CTRL	Rep2	pair-end	79206302	99.07	58423838	26.2	54837431	69.2	44402	0.1664
H3K27ac	ZT12	HFD	Rep1	pair-end	84552836	99.30	49329740	41.7	46049057	54.5	49453	0.1647
H3K27ac	ZT12	HFD	Rep2	pair-end	94871058	99.37	64956552	31.5	60929164	64.2	48979	0.1669

Table S4, related to STAR Methods. Static peak list used for IP efficiency normalization.

GR, Stat5, PPARα Chip-seq data				
Chromosome	Start	Stop	Gene	Location
chr1	74767896	74768942	<i>Cyp27a1</i>	intron-1
chr5	90878666	90879685	<i>Alb</i>	promoter
chr8	112527807	112528871	<i>Tat</i>	promoter
chr10	11000311	11001369	<i>Fbxo30</i>	promoter
chr10	41922139	41923197	<i>Foxo3</i>	intron-2
chr10	76553985	76555035	<i>Col18a1</i>	intron-2
chr15	31155792	31156844	<i>Dap</i>	intron-1
chr17	85092692	85093762	<i>Abcg8</i>	intron-5
chr18	64485085	64486104	<i>Onecut2</i>	promoter
chr18	64509730	64510838	<i>Onecut2</i>	intron-1
H3K27ac Chip-seq data				
Chromosome	Start	Stop	Gene	Location
chr12	105101829	105102829	<i>Serpina1b</i>	promoter
chr17	12570475	12571475	<i>Plg</i>	promoter
chr3	94690880	94691880	<i>Psmc4</i>	promoter
chr5	90888915	90889915	<i>Alb</i>	promoter
chr7	13620126	13621126	<i>Chmp2a</i>	promoter
chr8	112513336	112514336	<i>Tat</i>	promoter